Combining hydrodynamics, hydrochemistry, and environmental isotopes to understand the hydrogeological functioning of evaporite-karst springs. An example from southern Spain

J.M. Gil-Márquez*, B. Andreo, M. Mudarra

Department of Geology and Center of Hydrogeology of the University of Málaga, Faculty of Science, Málaga, E-29071, Spain

*Corresponding author: Tel.: +34 951952952, E-mail address: josemgil@uma.es

orcid.org/0000-0002-6318-6231

Keywords: evaporite karst – hydrogeochemical processes – hydrodynamics – tritium - S Spain

1. Introduction

The importance of karst aquifers can be traced to ancient civilizations (e.g. Greek, Roman, Persian or Chinese empires) that used karst springs for water supply in many cities and villages (LaMoreaux, 1999; Parise & Sammarco, 2015). Karst water exploitation has continued for centuries, and approximately 15%-25% of the world´s population relies on it nowadays (Ford & Williams, 2007; Stevanovic, 2018). In some European countries and in southwest China, karst resources represent over half of the freshwater supply (EU, 1995; Chen et al., 2017). A better understanding of the inherent hydrological complexity of these aquifers is needed to advance in the implementation of sustainable water governance strategies, particularly in Europe (EU, 1995, 2004). Researchers and administrations contribute to this progress by

developing and applying numerous karst-specific approaches (Goldscheider & Drew, 2007, and references therein), which shed light on the functioning of aquifers and their available water resources. Hydrogeological interest in evaporite karst systems is traditionally minor, as their groundwater resources are usually not suitable for drinking, due to their high solute contents (Andreo et al., 2016; D'Angeli et al., 2017).

Evaporite rocks are extensively spread worldwide, being present on roughly 25% of the Earth´s continental surface (Klimchouk et al., 1996). The largest evaporite outcrops are found in North America and Russia (Warren, 2016), although abundant literature focuses on other European and Asian countries, such as Spain (Calaforra et al., 2002; Gutiérrez et al., 2008a; Acero et al., 2015), Italy (Parise & Trocino, 2005; Buchignani et al., 2008; De Waele et al., 2017), Ukraine (Klimchouk & Aksem, 2005; Hryniv et al., 2007), Albania (Velaj, 2002; Parise et al., 2008), Turkey (Kaçaroğlu et al., 2001; Apaydin & Aktaş, 2012), or Iran (Raeisi, 2013; Naderi et al., 2016; Bruthans et al., 2017). Typically, research on evaporites looks into speleogenesis (Parise & Trocino, 2005; Calaforra, et al., 2008; Klimchouk, 2012; Di Maggio et al, 2012; De Waele & Pasini, 2013; Sanna et al., 2015; Columbu et al., 2015; De Waele et al, 2017) and natural or human-induced geohazards (Buchignani et al., 2008; Gutiérrez et al., 2008b, 2014; Parise, 2010; Fidelibus, et al., 2011; Acero et al., 2015; Yechieli et al., 2016), because the high solubility of gypsum, anhydrite, and halite favors rapid formation of subsurface karst conduits, often resulting in collapse and subsidence phenomena. Aspects associated with the hydrogeology of evaporite karst formations are not so well known, even though their resources usually contribute to the hydrological functioning and preservation of groundwater-dependent ecosystems, including wetlands (Sullivan et al., 2013; Beltram, 2016) and rivers (Ford & Williams, 2007).

Wetlands related to evaporite outcrops are abundant and diverse (Andreo et al., 2016; Warren, 2016). They host such varied wildlife species that many have achieved international

relevance, such as Cuatrociénegas in México, Whooping Crane Summer Range in Canada**,** Al Wathba in the United Arab Emirates, Bazer-Sakra in Algeria, or Fuente de Piedra and Zoñar in Spain (Valero-Garcés, et al., 2006; Gutiérrez et al., 2008a; Cardona et al., 2018; Sathish et al., 2018). But the natural drainage of evaporite systems is often accompanied by a deterioration in the chemical quality of downstream water in rivers (Memon et al., 1999; Kaçaroglu et al., 2001; Phillips et al., 2003; Négrel et al., 2007), dam reservoirs (Carrasco, 1986; Calaforra et al., 2002; Miyamoto et al., 2007; Aghdam et al., 2012; Raeisi et al., 2013) and even freshwater aquifers (Apaydin & Aktaş, 2012; Naderi et al., 2016). Thus, there are compelling reasons to perform research and develop scientific strategies that could help us to understand particular details of the hydrological functioning of evaporite karst systems.

Heretofore, most publications dealing with the hydrogeology of evaporite formations provide an overview of their general characteristics (Johnson, 1985; Pulido-Bosch & Calaforra, 1993; Klimchouk, 1996; Andreo et al., 2016; Nekouei & Zarei, 2017), or the geochemical processes behind groundwater salinization, or the geomorphological evolution of evaporitic karst areas (Mehta et al., 2000; Omelon et al., 2006; Acero et al., 2015; Gue et al., 2015; Qi et al., 2018). Few research efforts apply scientific strategies based on the integration of techniques specific to karst hydrogeology: continuous records of natural responses, hydrochemistry, environmental isotopes, dye tracers, etc. Some authors (Chiesi et al. 2010; Vigna et al. 2017; D'Angeli et al., 2017) have explored this approach, combining spring time series analyses of discharge rate, water temperature, and electrical conductivity, yet without equal consideration of chemical and isotopic parameters. Recently, Frank et al. (2019) analyzed major ion time series during a single flood in a gypsum karst spring located in the Austrian Alps, a means of inferring the importance of conduit-matrix interaction in the system´s workings.

There is clearly room to further investigate the hydrogeological functioning of evaporite karst systems by including information from other sources and characterizing techniques. The

present goal is to arrive at a realistic understanding of flow patterns and evaluate the main geochemical processes involved. Recent studies (Andreo et al., 2016; Gil-Márquez et al., 2017a; b) highlight the hydrogeological complexity of certain evaporitic systems, including hierarchically organized groundwater flowpaths of different lengths and residence times, from quick and shallow local flows through karst conduits to deep, diffusive, and slow regional flows. Combining information obtained from as many experimental methods as possible, with a joint interpretation of results, would allow researchers to define specific actions to be applied for the management and protection of wetlands associated with evaporite formations. It would also help mitigate the negative effects of brine groundwater on the quality of water resources (rivers, reservoirs, aquifers) downstream.

The value of springs as exceptional observation points and integrators of the whole drained system is widely acknowledged by the scientific community (Birk et al., 2004; Hunkeler & Mudry, 2007; Barberá & Andreo, 2011; Hartmann et al., 2014; Sánchez et al., 2015; Filippini et al., 2018). Detailed monitoring and analysis of their natural responses, often reinforced by other techniques (dye tracing, environmental isotopes - $\delta^{18}O$, $\delta^{2}H$, ^{3}H -, intrinsic fluorescence), shed new light on the idiosyncratic functioning of karst aquifers (Smart & Worthington, 2004; Goldscheider & Drew, 2007), and more specifically, of their infiltration processes, the groundwater flow velocity, residence times and location of storage (epikarst, unsaturated or saturated zones), and the degree of participation of these zones in the workings of the entire karst system (Hunkeler & Mudry 2007; Mudarra et al., 2011). Deductions may be supported by statistical treatment to interpret results and reinforce conclusions, e.g. Principal Component Analysis (PCA) or trend analysis (Bakalowicz, 1979; Mudry & Blavoux, 1987; Reisenhofer et al., 1998; Helsel & Hirsch, 2002; Stuart et al., 2007).

In this study, a brine spring (Lower Anzur; TDS ≃ 140-160 g/l) located at the border of an evaporite karst plateau in S Spain was studied. It was monitored for four hydrological years

(September 2013–October 2017) as a pilot site to investigate the hydrogeological behavior of evaporite karst systems in temperate climatic conditions. This outlet has significant environmental and social implications, as it drains groundwater with high solute content, annually transporting about 20,000 tons of NaCl (Gil-Márquez, 2018). The water drained by the spring, together with the surface runoff water flowing into the nearby Anzur River, is retained by a dam some 15 km downstream. Consequently, the reservoir water is brackish and cannot be used for urban supply, only for energy generation and irrigation purposes. There are moreover several endorheic areas in the catchment area of the pilot evaporitic system, many constituting ephemeral lakes and groundwater-dependent wetlands of variable size but of great environmental value (some listed in the Ramsar Convention of Wetlands). On the whole, the system drained by the Lower Anzur spring is of vast scientific interest, given its geological and geomorphological characteristics, with diverse lithologies and chaotic structure, which determine its hydrogeological complexity, including diffuse and conduit flow behaviors (Andreo et al., 2016).

The aim of this work is to enhance our knowledge of the hydrogeological functioning of evaporite karst systems by applying and analyzing the results obtained from routine monitoring of the natural response of a karst spring (Lower Anzur). Time series of discharge rates, physico-chemical data (e.g. electrical conductivity and water temperature), major dissolved ions, and isotopic signature were taken into account. Statistical treatment of the obtained dataset, jointly analyzed with information derived from intrinsic fluorescence and tritium (^{3}H) determinations, among others, led us to new insight into the hydrogeological processes controlling the hydrodynamic and hydrochemical variations in the outlet. Based on these results, a hydrogeological conceptual model of the system was constructed. The ultimate aim would be to achieve a comprehensive understanding of groundwater flow behavior, to be applied for water planning policies and the management of natural areas and regional water resources.

2. Location, climate, geological and hydrogeological setting

The Jarales site (Fig. 1) is an evaporitic karst plateau of approximately 80 km^2 located between two rivers in southern Cordoba province (Andalusia, Spain): the Genil (southwards) and its tributary, the Anzur (to the north). The area ranges from 250 to 450 m a.s.l., and the land is predominantly covered by extensive olive orchards, characterized by bare soil. The prevailing climate is temperate Mediterranean, with an uneven annual rainfall distribution, mainly taking place from autumn to spring (very often stormy). The mean air temperature in Jarales is 17.2ºC, while the historic annual rainfall (1963-64 to 2015/16) amounts to 508 mm (Gil-Márquez, 2018). During the study period, between the hydrological years 2013/14 and 2016/17, the annual precipitation ranged from 324 mm in 2014/15, to 403 mm in 2015/16. Thus, our research was carried out in clearly dry years, though the previous ones were quite wet, with up to 821 annual rainfall in 2012/13, and 913 mm in 2009/10 (Gil-Márquez, 2018).

From the geological standpoint, the Jarales area belongs to the Chaotic Subbetic Complex (CSC), a geological unit that extends along the northern sector of the so-called Subbetic Domain in the Betic Cordillera. The CSC is essentially a megabreccia made up of multi-colored Triassic (Keuper) clays and evaporite rocks (gypsum, anhydrite and halite), in addition to blocks of other ages and diverse lithology, including Triassic and Jurassic carbonates, Cretaceous marls and Miocene sandstones (Vera & Martín-Algarra, 2004). Gypsum can be found as massive rock or forming polygenic breccias. Though halite is absent at the surface as a consequence of its high solubility, its existence at depth is deduced from the existence of brine springs draining the evaporitic system (Andreo et al., 2016) as well as from some exploration boreholes (Carrasco, 1986, Calaforra & Pulido-Bosch, 1999). The CSC underwent massive gravitational displacement during Alpine orogeny and is consequently highly deformed (Pérez-López & Sanz de Galdeano, 1994). The original stratigraphic relationships are therefore seldom preserved.

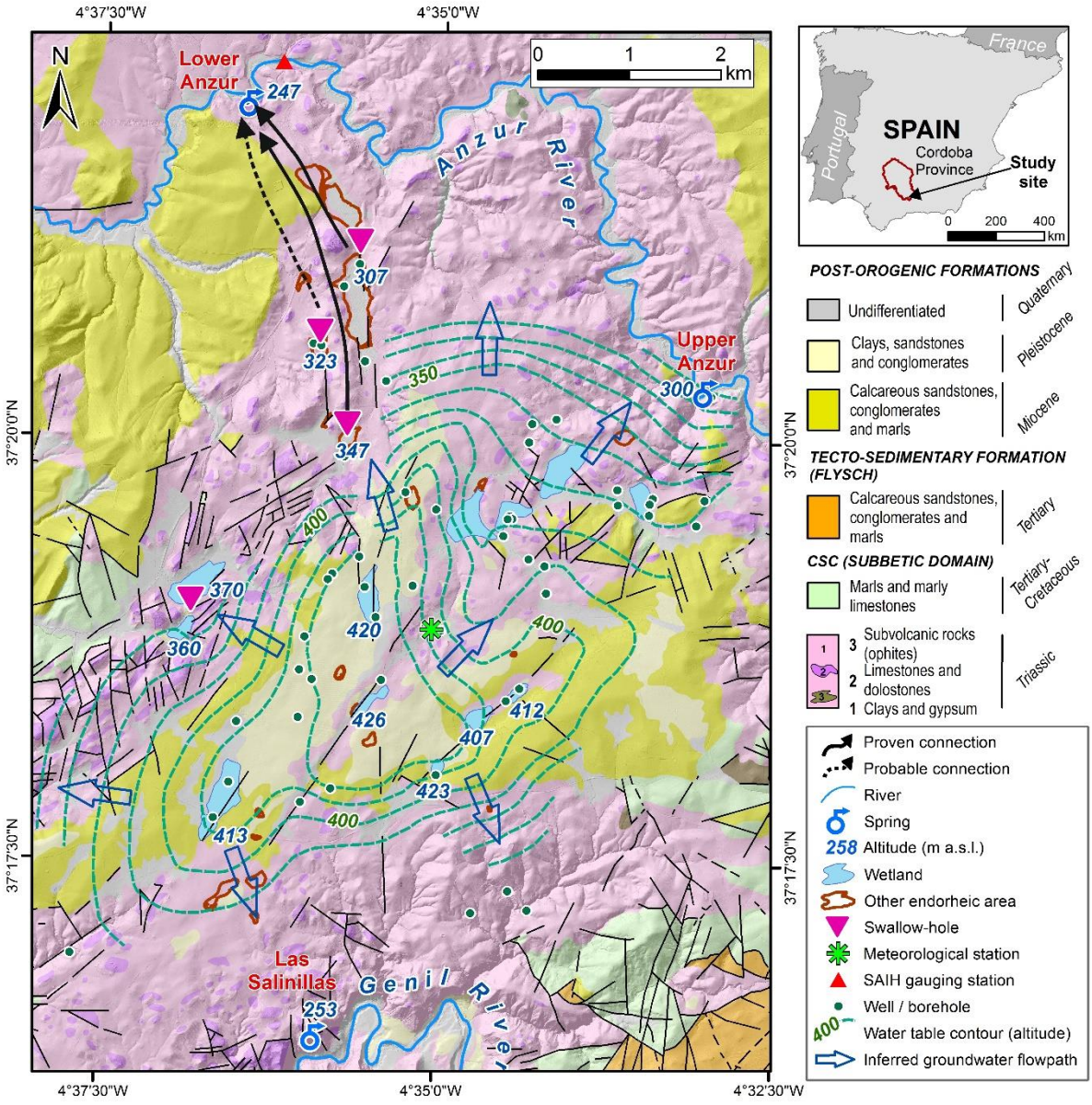

Figure 1. Geographic location and geological-hydrogeological sketch of Jarales Area (Córdoba Province, S Spain). Modified from Martín-Serrano (1986) and Divar et al. (1988). Hydrogeological connections deduced from tracer test results (Gil-Márquez et al., 2017a) and a sketch of groundwater table contours (Andreo et al., 2016) are also represented.

From a geomorphological standpoint, the study site is characterized by gentle hills, a poorly defined drainage network, and the existence of karst landforms related to the dissolution of evaporite rocks. The most remarkable exo-karst features are endorheic areas (closed depressions), some of which host wetlands of diverse size (Fig. 1) and variable hydroperiod (i.e. flooding duration) as a result of hydraulic interactions with the subsurface water table. In

158 the northern sector of the study area, the karst depressions are naturally drained through
159 swallow holes (Fig. 1), although their drainage capacity is limited, giving rise to occasional
160 flooding during wet periods (Gil-Márquez et al., 2017a).

161 Besides direct infiltration of runoff into swallow holes, recharge is also produced by diffuse
162 infiltration of rainwater through permeable outcrops (gypsum, carbonate rocks), and probably
163 through the bottom of wetlands and other endorheic depressions (Andreo et al, 2016; Gil-
164 Márquez, 2018). Given the abundance of clay lithologies, the CSC presents a general aquitard
165 behavior and groundwater predominantly flows within a diffuse-type system. Based on water
166 local table measurements, flow lines are drawn in a radial divergent pattern, from the central
167 part of the plateau at higher positions, to its borders (Fig. 1) at lower ones. Thus, natural
168 discharge takes place via springs located close to the Anzur and Genil rivers.

169 Although groundwater discharge is related to a diffuse flow system, the outlets also show
170 quick natural responses to recharge that are characteristic of karst aquifers. This is even more
171 remarkable in the Lower Anzur spring, where a high variability of discharge rate and physico-
172 chemical components has been registered (Gil-Márquez, 2018). A dye tracer test performed in
173 2016 (Gil-Márquez et al., 2017a) demonstrated the hydraulic connection between two karst
174 swallow holes and the outlet (Fig. 1), with a maximum flow velocity of 192 m/h. Additionally,
175 the alignment of karst features along the N-S direction suggests a high development of the
176 conduit network in the northern part of the system, making possible a hydrogeological
177 connection between other karst depressions and the Lower Anzur spring.

178 ## 3. Methods

179 ### *3.1.* Field measurement and sampling

180 A gauging station with a 60º V-notch weir was equipped in the Lower Anzur spring. Hourly
181 records of water temperature (T), electrical conductivity (EC), and water level variations in the

spring were registered from February 2014 to September 2017. EC and T were logged using a WTW® 350i multi-parameter measuring instrument, while water level lectures were recorded by an Odyssey® depth and temperature data-logger (~1 mm accuracy) for the continuous discharge record. The evolution of discharge rate was obtained by applying the rating curve of the gauging station (Gil-Márquez, 2018) to the water level variation series. Occasionally, rises in the Anzur River produced complete flooding of the outlet area. The runoff effect on the spring gauging station was deleted thanks to the flow rate data series registered 600 m upstream in the Anzur River (Fig. 1) by the automatic hydrologic information system (SAIH) of the Guadalquivir River Basin Authority. *In situ* measurements of discharge rate (OTT® C2 Flow Meter), EC and T (WTW® Cond 3310) were also carried out in the Lower Anzur spring, from September 2013 until the end of the study period. The measurement accuracies were ±2% for flow rate, ±0.1 mS/cm for EC, and ±0.1ºC for water temperature.

Concurrently, water samples (132) were collected in 150-ml amber glass bottles for subsequent chemical and isotopic analyses in the laboratory. Measurement and sampling periodicity were adapted to the hydrological conditions of the system (recharge, recession, depletion): from several times per day in high flow conditions, to monthly during depletion periods. Additionally, five spring water samples were taken in 1-litre PET bottles for tritium determination, from September 2014 to December 2016, under diverse hydrodynamic conditions.

3.2. Analytical methods

Samples were mainly processed in the laboratory of the Centre of Hydrogeology of the University of Malaga (CEHIUMA). HCO_3^- was determined by volumetric titration with 0.02 N H_2SO_4 to pH 4.45 (Metrohm™ 888 Titrando). Major ions (Ca^{2+}, Mg^{2+}, Na^+, K^+, Cl^-, SO_4^{2-}, NO_3^-) were analyzed using high-pressure liquid chromatography (HPLC Metrohm™ Compact 930 IC Flex for cations and Metrohm™ Compact 881 IC pro for anions) with 2% accuracy.

Due to their high solute content, samples were diluted to 1 mS/cm and filtered (0.45 µm Millipore® filters) before their introduction in the system (filter in line and precolumn-filter). The accuracy of the chemical data was checked using the Charge Balance Error (CBE), calculated as the difference among the sums of the equivalent concentrations of anions and cations (Σcations - Σanions) divided by the sum of equivalent concentrations of all ions (Σcations + Σanions). The mean CBE value for the whole sample set was 2.5 %, and samples with CBE outside ±5% were discarded.

Intrinsic fluorescence of samples is produced by dissolved organic matter, and its presence in groundwater allows one to study recharge in karst aquifers (Birdwell and Engel, 2007). It was analyzed using a Perkin-Elmer^{TM} LS55 spectrofluorometer. The excitation-emission matrices (EEMs) were obtained by means of the simultaneous scan of excitation and emission wavelengths from 200-350 and from 250-550 nm, respectively, with intervals of 5 nm. In both cases, a 5 nm slit was used with a scanning rate of 500 nm/min. The Raman peak of deionized water, measured at an excitation wavelength of 348 nm and with emission monitored at 390-395 nm, was used to determine the stability of the instrument (Lawaetz & Stedmon, 2009). The maximum fluorescence intensity of each peak was therefore referred to as Raman units (RU). Peak A, produced by humic acids, appears between 230 and 250 nm excitation wavelengths and from 405 to 445 nm emission wavelengths, whereas peak C, related to fulvic acids, is found between excitation wavelengths 300-335 nm and emission wavelengths 400-440 nm.

Water isotopes ($\delta^{18}O$ and $\delta^{2}H$) were determined by means of isotope-ratio mass spectrometry (IRMS) in the central laboratory of the University of Malaga (SCAI). Corrected data were referred to the Vienna Standard Mean Ocean Water (VSMOW). Due to the fractionation between free water molecules and those associated with the hydration sphere of cations in water solution, the isotope activity ratios of brine samples differ from their isotope concentration ratios (Taube, 1954; Horita, 1989). Hence, $\delta^{18}O$ and $\delta^{2}H$ data were converted

from activity scale to concentration scale by applying the "activity correction" defined by Sofer and Gat (1972, 1975):

$$\Delta\delta\ ^{2}H = mNaCl(0.4) + mMgCl_2(-5.1) + mCaCl_2(-6.1) + mKCl(-2.4)$$

$$\Delta\delta^{18}O = mMgCl_2(1.11) + mCaCl_2(0.47) + mKCl(-0.16)$$

where *m* is the molality of the respective ions and $\Delta\delta^{18}O$ and $\Delta\delta^{2}H$ are the "activity corrections", which are the differences between the δ-values on the concentration scale and those on the activity scale.

Tritium (^{3}H) analysis was carried out in the Department of Oceanography of the Institute of Environmental Physics, University of Bremen, based on the ^{3}He–ingrowth method (Clarke et al., 1976). First, 500 g of degassed water samples were stored in gas-free glass bulbs for the production and accumulation of ^{3}He, the decay product of ^{3}H. After 4-6 months of storage, ^{3}He was extracted from each sample and then separated from any other remaining or generated gases by means of a cryogenic system. The ^{3}He concentration was determined with the mass spectrometric system, described in detail by Sültenfuß et al. (2009). The specific radioactive activity of ^{3}H is expressed in Tritium Units (TU = 0.119 Bq/kg of H_2O). In order to make ^{3}H values in groundwater samples comparable to those in precipitation, the content of ^{3}H determined in each sample was corrected according to its density (enhanced by the high mineralization) and then expressed as a concentration in freshwater. Water sample density and ion molalities, used for salt correction of the isotope data, were obtained based on their chemical composition, using the software PHREEQC (Parkhurst & Appelo, 2013) and the PITZER geochemical database (Plummer et al., 1988).

3.3. Data processing

The statistical treatment of the hydrochemical dataset was performed by means of the software XLSTAT v.7.5.2 by ADDINSOFT™. Principal component analysis (PCA) was

applied to aid interpretation of the hydrochemical response of the spring. This method, broadly used in karst hydrogeology (Bakalowicz, 1979; Mudry & Blavoux, 1987; Reisenhofer et al., 1998; Hunkeler & Mudry 2007; Barberá & Andreo, 2011; Sánchez et al., 2015), makes it possible to reduce the variance of multidimensional data sets by means of principal components or factors (Melloul & Collin, 1992).

To identify any significant trend in the natural responses of Lower Anzur spring during the study period, the nonparametric Mann-Kendall test (Mann, 1945; Kendall, 1975) was applied to the monthly data series of major dissolved ions, EC and T, as well as to the series obtained from the hourly records of EC and T. This procedure is widely used to assess the existence of chemical trends in hydrological and hydrogeological studies (Helsel & Hirsch, 2002; Yue & Wang, 2004; Stuart et al., 2007; Wahlin & Grimval, 2010; Merchán et al., 2013; Urresti-Estala et al., 2016). The test statistics (τ and S) indicate rising trends when positive, whereas they reveal downward tendencies if negative. The general variation of each parameter was quantified by Sen's slope test (Sen, 1968; Hirsch et al., 1991), it being less affected by major data error or outliers than linear regression methods. Sen's slope values are expressed as units of the analyzed parameter according to the periodicity of the time series, and they were used to calculate the annual trend of each parameter. Only those analyses with a p-value less than or equal to the significance level (α) of 0.05 were considered statistically significant.

4. Results

4.1. Hydrodynamics

The discharge rate of Lower Anzur spring varied from less than 1 l/s to nearly 100 l/s, with an average value of approximately 5 l/s (Tab. 1). The spring hydrograph (Fig. 2A) shows several floods per year in response to recharge events. In general terms, discharge peaks were sharp and occurred rapidly, a few hours after the onset of rain. Differences in the magnitude of

discharge fluctuations were observed, depending on the amount and intensity of rainfall and also on the previous hydrodynamic conditions of the system (Fig. 2). Thus, the first recharge episodes of each hydrological year (October) generally gave rise to flow peaks in the order of 30-40 l/s, while volumes up to 80-90 l/s were reached as a response to other significant precipitation events occurring in autumn or winter (Fig. 2A) and having a greater magnitude or occurring during recession. The corresponding decreases in discharge also took place very quickly, whereas slow variations were recorded under depletion conditions.

	Discharge rate		EC		T														
	Single data	Cont. Record	Single data	Cont. Record	Single data	Cont. Record	HCO_3^-	Cl^-	NO_3^-	SO_4^-	Ca^{2+}	Mg^{2+}	Na^+	K^+	A peak	C peak	$\delta^{18}O$	δ^2H	^3H
n	90	29,015	131	27,052	131	27,052	132	127	116	117	129	129	129	129	57	57	30	7	5
med	5.1	4.6	148.8	154.5	20.7	20.5	241	86,243	21	6,004	2,290	418	54,087	218	17.7	8.6	-6.1	-36.1	2.0
máx	92.0	98.8	167.8	168.5	21.6	21.6	268	113,581	85	8,326	3,621	720	70,000	298	43.0	20.5	-5.5	-33.4	2.6
mín	0.7	0.2	120.6	117.5	19.4	18.2	185	63,105	0	4,907	1,751	246	39,464	159	10.7	5.5	-7.1	-40.0	1.1
cv	140	223	8	18	2	2	9	12	91	10	9	19	12	14	36	36	8	6	28

Table 1. Main statistical descriptors (n, number of samples/measurements; min, minimum; max, maximum; mean, average; and cv, coefficient of variation %) of discharge rate and physicochemical data from Lower Anzur spring water. Units: discharge rate in l/s, electrical conductivity (EC) in mS/cm, water temperature (T) in °C, major ions in mg/l, A and C peaks in Raman Units (RU), $\delta^{18}O$ and δ^2H values in ‰ VSMOW (Vienna Standard Mean Ocean Water), ^3H in tritium units (TU).

The four unitary hydrographs displayed in Figure 2 correspond to some of the greatest flood events of the hydrological years 2014/15 and 2015/16. For each, the response lag-time to the recharge event (t_L) and the flood base time (t_B) were calculated (Tab. 2). The first flood (Fig. 2B) started under recession conditions, three days after a previous flood (Fig. 2A). Outflow rose up to 80 l/s in 19 h (t_L) as a response to 22 mm of precipitation within 24 hours. Recession started slowly afterward, but it accelerated below 70 l/s. The flood base time (t_B), from the beginning of the rising limb to the start of depletion, was 4 days. Two weeks later, 9 mm of precipitation caused a discharge peak of 66 l/s (Fig. 2C & Tab. 2) The t_L was 22 h and the recession started rapidly after the peak. During the study period, the highest discharge value (99 l/s) was recorded in November 2015 (Fig. 2D & Tab. 2) after the heaviest precipitation event registered (43 mm within 6 h). The t_L was 40 h, while t_B lasted 6 days. The recession limb

was gentle during the first three days, then started to decrease rapidly after the discharge value reached 67 l/s. The last unitary hydrograph analyzed (Fig. 2E & Tab. 2) had a peak of 51 l/s after a 22-hour t_L, in response to 13 mm, and the recession was quick.

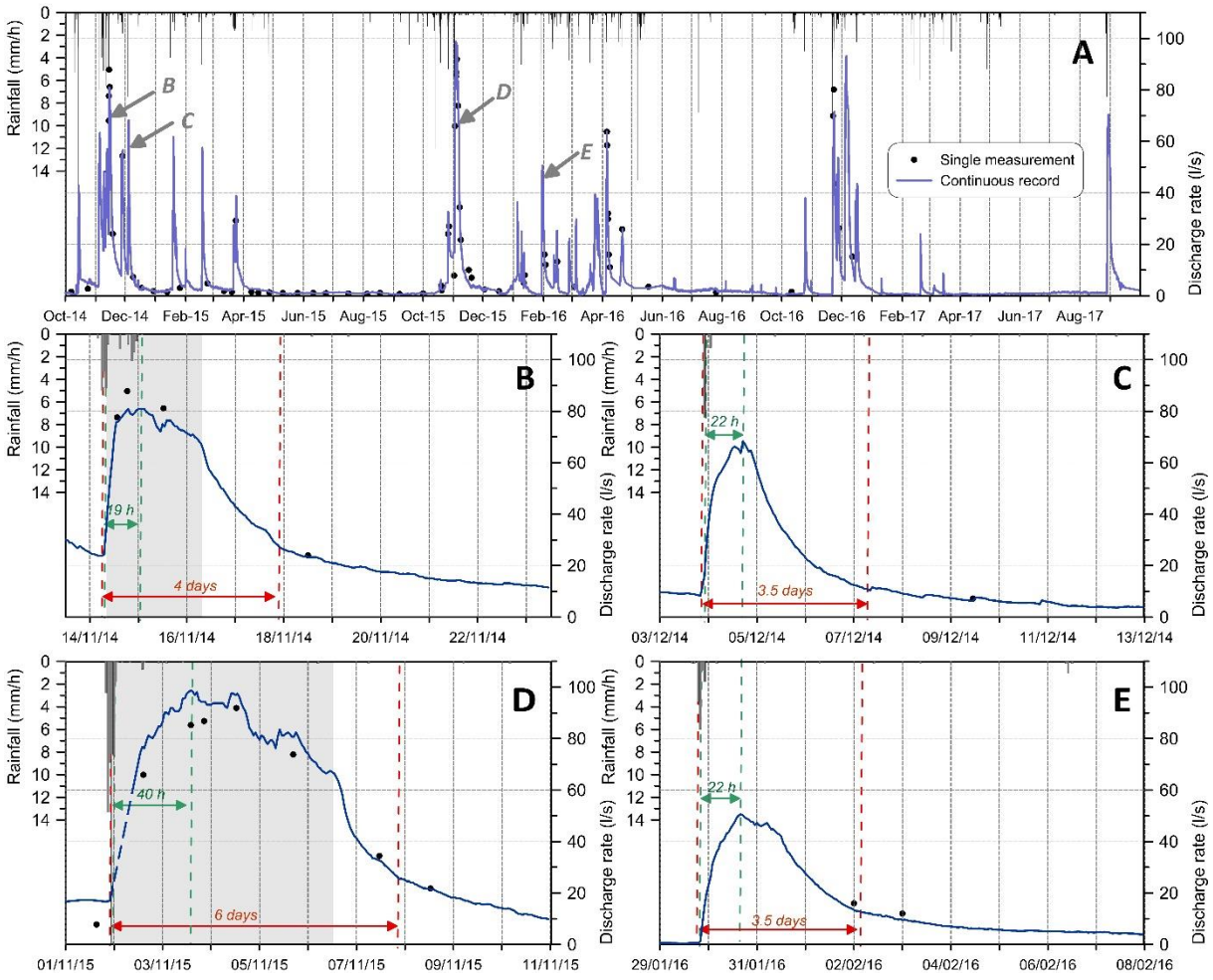

Figure 2. Lower Anzur spring hydrograph and daily precipitation, from October 2014 to September 2017 (A), and some unitary hydrographs (B-E). Response lag-time (t_L) and flood base time (t_B) are indicated in green and red, respectively. Shaded areas in B and D show the periods during which exokarstic depressions with swallow holes were flooded. The dashed line in hydrograph D indicates data completed by linear interpolation, due to flooding of the gauging section during Anzur River flow rising.

Date	Flow peak (l/s)	t_L (hours)	t_B (days)	Rainfall amount (mm)	Rainfall duration (h)
Nov. 2014	80	19	4	22	24
Dec. 2014	66	22	3.5	9	4
Nov. 2015	99	40	6	43	6
Jan. 2016	51	22	3.5	13	6

Table 2. Hydrodynamic data of four of the main floods in Lower Anzur spring.

315 ***4.2. Hydrochemistry***

316 Table 1 summarizes the most significant statistical parameters of the physicochemical
317 variables controlled in the Lower Anzur spring during the study period. The clear prevalence
318 of Cl^- and Na^+ facies (up to 113.6 and 70.0 g/l, respectively) defines the hypersaline nature of
319 the water drained by the outlet, with an average EC value of 154.5 mS/cm (continuous record).
320 Spring water also presented high mean contents of other ions, such as SO_4^{2-} Ca^{2+}, and K^+, while
321 HCO_3^- and Mg^{2+}, whose presence may be partially linked to evaporitic sources, had lower
322 concentrations (Table 1). The mean value of NO_3^- is 21 mg/l, although it varied notably
323 (cv = 91%), as did fluorescence peaks A and C (cv = 36%). The continuous record of water
324 temperature ranged from 18.2ºC to 21.6°C, a few degrees above the mean annual air
325 temperature at the pilot site (17.2 °C; Gil-Márquez, 2018).

326 The time series of the hydrochemical parameters measured in the water drained by Lower
327 Anzur spring during the study period are displayed in Figure 3, together with the spring
328 hydrograph and the daily rainfall recorded in a meteorological station located in the center of
329 Jarales area (Fig. 1). Great variability of the chemical composition of the spring water under
330 different hydroclimatic situations is observed, although generally increasing trends in some of
331 the controlled parameters were also recorded. Observing depletion periods, water
332 mineralization and EC increased, from values around 145 mS/cm at the end of 2013, to
333 approximately 165 mS/cm in the summer of 2017. Meanwhile, the range of water temperature
334 rose from 20.1-20.8ºC in hydrological year 2013/14, to 20.4-21.5ºC in 2016/17. Such variations
335 were statistically analyzed by means of the Mann-Kendall test and Sen's Slope (Table 3).
336 Upward trends were identified in the series of EC, T, Cl^-, Na^+, and K^+. Sen's slope indicates
337 that EC rose 4.35-4.59 mS/cm annually, while T increased between 0.12ºC and 0.16ºC each
338 year. The greatest variation in mineralization was related to the increase of Cl^- (1,710 mg/year)
339 and Na^+ (3,566 mg/year) contents.

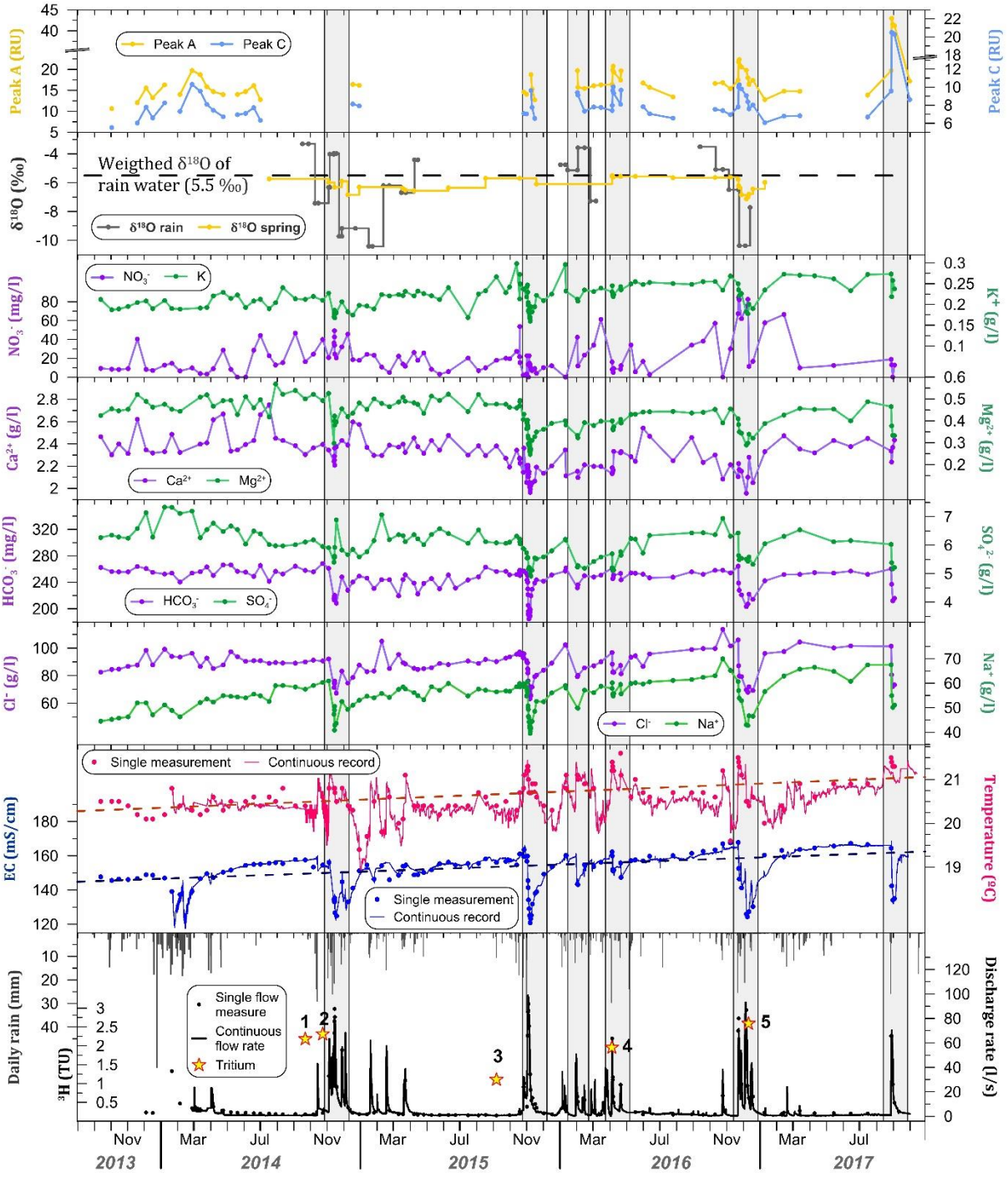

Figure 3. Time series of discharge rate, electrical conductivity (EC), temperature, major chemical components, intrinsic fluorescence of peaks A and C, and $\delta^{18}O$ values. Daily rainfall and $\delta^{18}O$ of rain samples and ^{3}H activity of five samples are also included. Shaded areas are shown in detail in Figure 4.

The general hydrochemical evolution trends were disrupted in each recharge period by quick and sharp falls in water mineralization. The magnitude of these dilutions depends directly on the amount and the intensity of rainfalls (Figs. 3 & 4). Variations in EC were clearly determined by changes in Cl^- and Na^+ concentrations, which evolved analogously to EC. In

addition, SO_4^{2-}, HCO_3^-, Mg^{2+}, Ca^{2+}, and K^+ contents followed relatively similar patterns to that of EC, whose values decreased during floods (Fig. 3). The temporal evolution of NO_3^- did not follow a clear pattern, its concentration showing variable behavior during flood peaks. In fact, in November 2015 and August 2017, coinciding with great flood events, NO_3^- was not detected in the samples, probably due to the magnitude of the dilutions. Water temperature presented slight fluctuations at low water conditions, and significant and quick variations as a consequence of the main recharge events, characterized by rapid rises followed by lagged pronounced falls (Fig. 3). Finally, the intensity values of intrinsic fluorescence in the water samples were enhanced during the most significant floods (Fig. 3). In general terms, peaks A and C reached values near 20 RU and 12 RU, respectively. Yet in the flood event of August 2017, dilution was accompanied by much greater intensity values (peak A rose up to 43 RU and peak C up to 20.5 RU).

Statistical	EC continuous record	EC single measurements	T continuous record	T single measurements	Cl^-	Na^+	K^+
τ	0.586	0.583	0.255	0.583	0.333	0.556	0.556
S	15409	42	6702	42	24	40	40
p-value	< 1.E-04	< 1.E-04	< 1.E-04	< 1.E-04	0.024	1.E-04	1.E-04
Sen's slope	0.00050	0.38	0.000013	0.013	142.5	297.2	1.5
Annual trend	4.35	4.59	0.12	0.16	1710.4	3566.4	17.7

Table 3. Main statistical results derived from Mann-Kendall and Sen's slope tests. The annual trends are expressed as mS/cm (EC), ºC (T) and mg/l (major chemistry) per year.

A detailed illustration of the temporal evolution of the spring water chemistry during some significant flood periods is displayed in Figure 4. Prior to water dilutions, and coinciding with the flow rises, slight increases in spring EC of up to 6 mS/cm were observed (Fig. 4), which were much lower than the subsequent decreases, with maximum drops of nearly 40 mS/cm (November 2015; Fig. 4). Both the hydrodynamic and the hydrochemical responses took place rapidly, a few hours after the start of the precipitation event that originated them, but there was a lag between flood peaks and dilution peaks (Fig. 4). The latter normally occurred between 1 and 4 days after the former, depending on the magnitude of the recharge. Return to the initial

values of EC was much slower than the reestablishment of discharge rate, because the flow decrease was prolonged in a time interval of several days, while the mineralization recovery could take more than two months after the most pronounced dilutions (Figs. 3 & 4). In turn, the water temperature of the spring tended to be higher during flow peaks, when slight rises in water mineralization were recorded, and it fell as the spring moved into dilution conditions. Nevertheless, the minimum temperature values were reached once mineralization was almost recovered (Figs. 3 & 4).

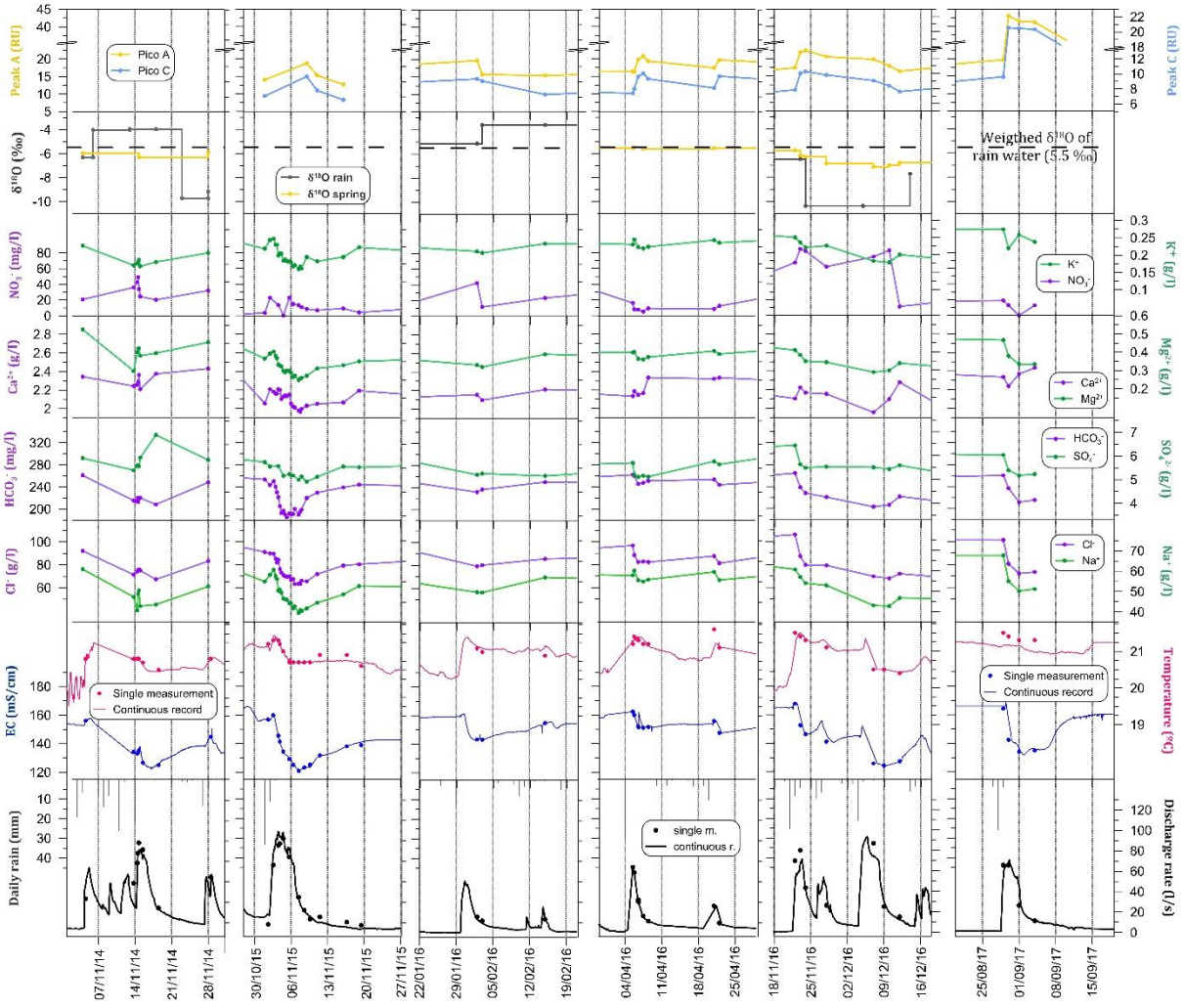

Figure 4. Detail of six different flooding periods recorded in Lower Anzur spring.

Based on the chemical data of the samples taken in Lower Anzur spring, a principal component analysis (PCA) was carried out, using the 10 variables in Table 4 whose series

showed a more continuous series (Fig. 3). The generated correlation matrix reflects a highly positive relationship (> 0.9) of EC with Cl^- and Na^+, and to a lesser extent with HCO_3^-, K^+, and Mg^{2+} concentrations. HCO_3^- is also correlated with Cl^- and Na^+. A positive relationship was also determined, to a minor degree, between each of the following: Cl^-, Na^+, K^+, SO_4^{2-}, and Mg^{2+}.

The two main factors of the PCA explain 71% of the hydrochemical variability of the sample set taken in Lower Anzur spring (Fig. 5). The first (F1, 54.93%) is defined by EC, Na^+ and Cl^-, which are the main chemical species related to EC, and, to a lesser extent, by HCO_3^-, Mg^{2+}, K^+, and SO_4^{2-} (Fig. 5A). Therefore, the first factor reflects water mineralization and residence time inside the aquifer. However, the variables that determine this factor are distributed in two different groups. The first group is situated towards positive values of F2 and is formed by EC, Na^+, Cl^- and HCO_3^-, which are the variables having a higher influence in F1, and K^+. This group would therefore be mainly related to the dissolution of halite (NaCl), sylvite (KCl) and carbonates. The second group has lower F1 values and is shifted to the negative side of F2. It is formed by Mg^{2+}, SO_4^{2-} and Ca^{2+}, derived mainly from the dissolution of gypsum, anhydrite and evaporite minerals bearing Mg^{2+}, such as epsomite ($MgSO_4 \cdot 7H_2O$) and hexahydrite ($MgSO_4 \cdot 6H_2O$), although the cations could also have their origin in calcite ($CaCO_3$) and dolomite ($CaMg(CO_3)_2$) forming the carbonate rocks. The second factor (F2; 16.06%) has a positive relationship with water temperature (Fig. 5A), which would be tied to drainage of the saturated zone and possibly to the ascent of deep flows, given that the spring has a slight positive thermal anomaly.

	EC	T	HCO_3^-	Cl^-	NO_3^-	SO_4^{2-}	Ca^{2+}	Mg^{2+}	Na^+	K^+
EC	**1**									
T	-0.031	**1**								
HCO_3^-	0.886	-0.020	**1**							
Cl^-	0.931	-0.069	0.826	**1**						
NO_3^-	-0.056	-0.086	-0.094	-0.066	**1**					
SO_4^{2-}	0.579	-0.384	0.492	0.706	0.002	**1**				
Ca^{2+}	0.312	-0.303	0.364	0.273	-0.046	0.438	**1**			
Mg^{2+}	0.652	-0.403	0.673	0.628	-0.061	0.716	0.660	**1**		
Na^+	0.910	0.021	0.821	0.887	-0.058	0.580	0.446	0.649	**1**	
K^+	0.733	0.131	0.639	0.721	-0.023	0.398	0.297	0.383	0.793	**1**

Table 4. Correlation matrix obtained from the PCA performed with the hydrochemical information collected in Lower Anzur spring during the study period.

Figure 5B shows the observations (i.e. water samples) in the factorial plane defined by F1 and F2, classified according to the hydrological year and the hydrodynamic state. The samples having greater mineralization are located on the positive side of the F1 axis, while those related to dilution processes are located on the negative side. Along with F2, the samples are distributed from top to bottom as their temperature decreases. In general terms, samples that correspond to depletion situations are well grouped, while those related to flood peaks and recessions present greater dispersion in the F1-F2 plane (Fig. 5B). Waters drained during the spring depletions are characterized by high mineralization, relatively low temperatures, and the greatest values of Ca^{2+}, Mg^{2+}, and SO_4^{2-} of the whole set of observations. Samples corresponding to floods can be observed in the upper right quarter of Figure 5 or scattered throughout its left half. Finally, samples taken during recessions show low mineralization, though with much variability, and a wide range of temperature values (Fig. 5B). Additionally, the classification of samples according to the hydrological year in the factorial plane allows the year-to-year hydrochemical evolution of the waters drained by the Lower Anzur spring to be evaluated. The progressive increase of EC and temperature values, statistically quantified with the Mann-Kendall Test and Sen's Slope (Tab. 3), is again seen in Figure 5, mainly in those samples taken during flood events, and above all in those taken during depletion times. From the first to the last year of observation, depletion samples are displaced from the lower right quadrant, more related to

Ca^{2+}, Mg^{2+}, and SO_4^{2-}, towards upper positions, where the variables EC, K^+, Na^+, Cl^- and HCO_3^- are situated.

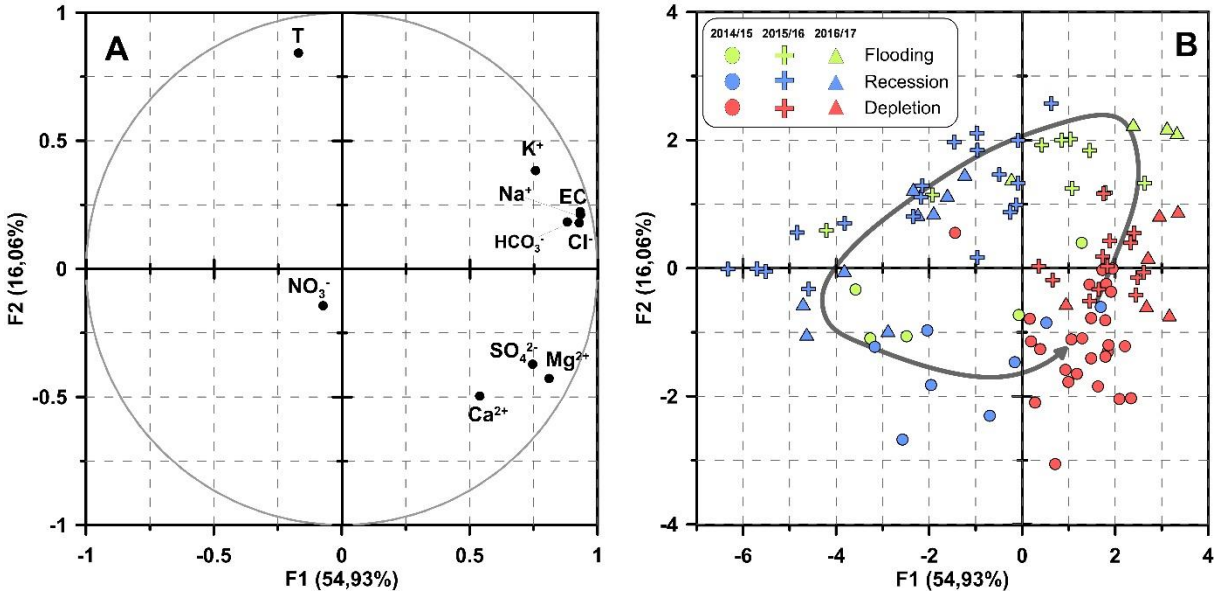

Figure 5. Factors 1 and 2 obtained from the principal component analysis (PCA) carried out with the main physicochemical parameters and major chemical components of the samples collected from Lower Anzur spring during the study period. Plots of the variables (A) and statistical units (B).

4.3. Isotope data

The $\delta^{18}O$ and $\delta^{2}H$ values of the Lower Anzur samples respectively ranged between -7.1‰ and -5.5‰ and from -40.0 to -33.4 ‰ (Table 1). Most samples taken during the summer season (Figs. 3 & 4), when no precipitation was recorded and therefore no recharge existed, had $\delta^{18}O$ contents very similar to the weighted average of $\delta^{18}O$ in the precipitation (-5.5 ‰) of the study area (Gil-Márquez, 2018). However, groundwater sampled during the greatest floods had lower isotopic values, such as in November and December 2016 (Fig. 3 & 4). The isotopic signature of the precipitation events that gave rise to significant spring floods produced a decrease in the $\delta^{18}O$ of the spring water, yet of more reduced magnitude.

The samples collected for tritium analysis were taken during diverse hydrodynamic conditions (yellow stars in Figure 3). Sample 1 was taken in September 2014, at the end of the summer depletion. Sample 2 was collected in October 2014 after the first recharge event of the

hydrological year 2014/15. Sample 3 coincided with another depletion period, September 2015. Finally, samples 4 and 5 were taken during two different stages of floods: a piston-flow effect (Nº 4) and a hydrochemical dilution (Nº 5).

Tritium was found in the five water samples analyzed, with values varying from 1.1 to 2.6 TU (Table 1), slightly lower than the available ^{3}H data of precipitation in the area during the study period, between 1.8 and 3.2 TU (Gil-Márquez, 2018), and the range of ^{3}H in the region (2-4) estimated by the Spanish Surveillance Network of Isotopes in Precipitation (Castaño & Rodríguez-Arevalo, 2019), which is part of the GNIP (Global Network of Isotopes in Precipitation). In Figure 6, ^{3}H concentrations in the groundwater samples are compared to the corresponding values of flow rate, water temperature, and EC. Generally, greater ^{3}H values were found when the discharge rate was higher and the water temperature was lower, although the relationship is stronger with the second parameter. The relation between ^{3}H and EC is less evident, but sample Nº 5 presented a higher isotopic activity and the lowest mineralization and water temperature (Figs. 6B & C), as it coincided with a hydrochemical dilution (Fig. 3). The other flood sample (Nº 4) was taken coinciding with rises in water temperature and EC, and it had the second lowest value of ^{3}H, 1.95 TU (Table 1). This last sample (Nº 4) decreases the correlation between flow rate and ^{3}H (Fig. 6A). However, the recession stage in the hydrogeological system, from dilution (flooding) to depletion, would be accompanied by a progressive decrease in the ^{3}H values (Figs. 5B & 6A).

5. Discussion and interpretation

The joint analysis of hydrodynamic, hydrochemical, hydrothermal and isotopic results described in the above section, together with the background information available from previous works (Gil-Márquez et al., 2017a; Gil-Márquez, 2018), has provided deeper insights into the structure and flow dynamics within the vertically distributed reservoirs (unsaturated and saturated zones) found in the evaporite karst system taken as the pilot site. The combined

treatment of the hydrogeological information also advances our understanding of the storage capacities and residence times of groundwater in the system, as well as in the water-rock interactions, and related hydrogeochemical processes. Quick rises in the flow rate after recharge events reveal the existence of a highly developed karst network, which permits fast flows and short transit time of groundwater within the system, from surface points of the epikarst where concentrated infiltration occurs (i.e. swallow holes) towards the spring. Similar behavior has been reported in other evaporite karst settings, where allogenic recharge likewise produces rapid hydrodynamic responses (Calaforra et al., 2002; Chiesi et al., 2010; Bruthans et al., 2017; D'Angeli et al., 2017; Vigna et al., 2017).

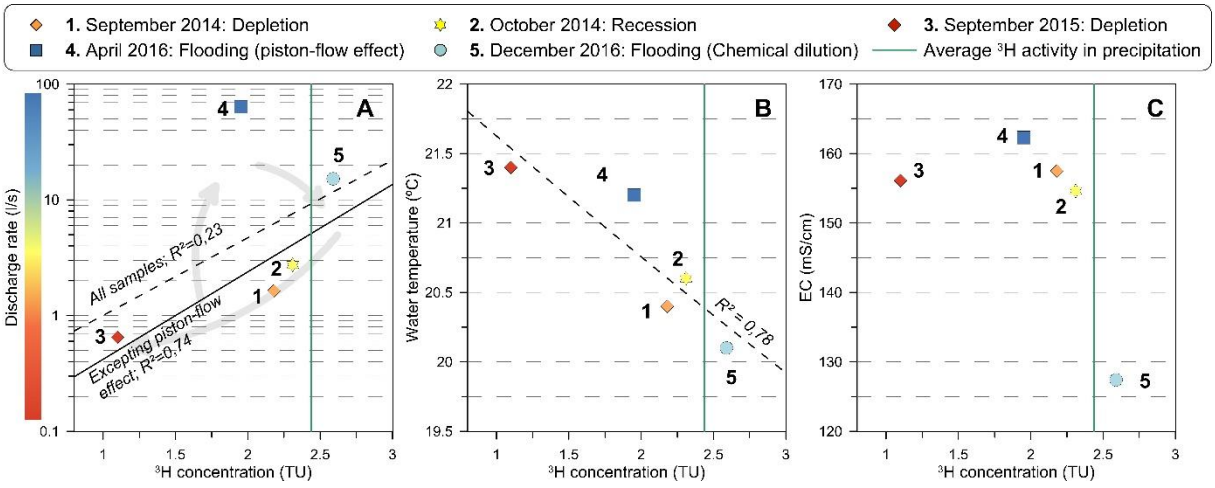

Figure 6. ^{3}H data of the groundwater samples collected in Lower Anzur spring vs discharge rate (A), water temperature (B) and electrical conductivity (C).

The morphologies of the hydrographs shown in Figure 2 are closely related to the maximum flow value drained in each case. The two major peaks considered (Fig. 2.B & D) present a relative flat shape that extends until the flow rate reached values below 70 l/s. This reference value is higher than those recorded in the other two floods periods (Fig. 2C & E), with better-defined peaks. The duration and flattening of the flow peaks coincided with periods in which the endorheic depressions (uvala and polje) south of the outlet (Fig. 1) —where karst swallow holes are located— were flooded. The decrease in discharge rate occurred more rapidly

when the flooding of the swallow holes was finished (Fig. 2.B & D), coinciding with a specific discharge value of approximetely 70 l/s. This, together with the absence of hydrograph flattening and the lack of flooding in karst depressions for lower flow, could suggest that the waterlogging of the swallow holes takes place due to a limitation of the karst network drainage capacity. A similar conclusion was deduced after analyzing the results from a multi-injection tracer test previously performed in the area (Gil-Márquez et al., 2017a). The existence of a narrow karst conduit network that becomes fully saturated in significant recharge events was inferred from that tracer experiment. Consequently, the flow of recently infiltrated water would be impeded, leading to the flooding of the endorheic areas. This in turn would produce a sustained recharge over time, giving rise to undefined flood peaks, which are often related to the existence of overflow springs (Bonacci & Bojanić, 1991; Barberá & Andreo, 2011; Malard et al., 2015) but are also characteristic of springs that are connected to the drainage of poljes (Bonacci, 1993; Ford & Williams, 2007), as is the case here.

The variations in water mineralization are mainly produced by changes in Cl^- and Na^+ contents, and to a lesser extent dissolved K^+; they evolve analogously to EC, and even presents a similar upward trend (Fig. 3 & Tab. 3). The positive correlation between both cations and Cl^- (Tab. 4) suggests that the source of these chemical species must be related to the existence of halite and sylvite (Hidalgo & Cruz-Sanjulián, 2001; Acero et al., 2015). On the other hand, the SO_4^{2-}, Ca^{2+}, Mg^{2+}, and HCO_3^- time series (Fig. 4) follow patterns relatively similar to that of EC, but they did not present an upward trend during the investigation period. The origin of SO_4^{2-} and Ca^{2+} is associated with the dissolution of gypsum, which is a part of the clayey-evaporite matrix that constitutes the CSC, though it is also present as massive gypsiferous bodies, where karst networks are better developed (Calaforra & Pulido-Bosch, 1999). However, SO_4^{2-} and Ca^{2+} present a poor correlation (Tab. 3), indicating that additional sources of one of these ions must exist. Thus, the content of Ca^{2+}, as well as those of Mg^{2+} and HCO_3^-, would be

linked to the dissolution of the carbonate olistoliths in the Jarales area (Fig. 1). Additionally, the high correlation between HCO_3^- and Na^+ and Cl^- indicates that the dissolution of carbonates is somehow related to the concentration of halite-derived solutes. The observed correlations can be explained by the effect of high ionic strength solutions (e.g. brine water) that enhances calcite solubility (Mucci, 1983; Appelo & Postma, 2005). Lastly, the relatively high correlation between SO_4^{2-} and Mg^{2+} could be caused not only by the dissolution of evaporite minerals but also from dedolomitization (Wigley, 1973).

Therefore, the first group of variables (EC, Cl^-, Na^+, K^+, and HCO_3^-) related to F1 in the PCA (Fig. 5A) would be related to groundwater flowing in deep areas within the saturated zone of the system. This is in agreement with the absence of halite and sylvite in outcrops and in explored karst conduits near the surface (Calaforra et al., 2002; Aljama-Martínez, 2017). Besides, this group of variables is situated towards positive values of F2 (defined by water temperature). The ascent of relative deep flows would explain the positive thermal anomaly observed in the spring water. To the contrary, the rest of the chemical variables that define F1 (SO_4^{2-}, Mg^{2+}, and Ca^{2+}) have a negative factor loading in F2. Hence, they could proceed from the whole system (both saturated and unsaturated zones), their presence in groundwater being explained by the dissolution of rocks that are present in surface and at depth.

Records of EC, water temperature, and most of the main dissolved ions generally showed lower values after recharge events (Fig. 3 & 4) and higher ones during depletion conditions. Such chemical dilution and water cooling are caused by the arrival of recently infiltrated water through swallow holes, as suggested by recent infiltration tracers. Intrinsic fluorescence of the organic matter from the soil is considered as a natural recharge tracer in carbonate aquifers (Birdwell & Engel, 2007; Lapworth et al., 2009; Mudarra et al., 2011). The quick rises of A and C fluorescent peaks (related to organic matter of edaphic origin) during chemical dilutions (Fig. 3 & 4) demonstrate that runoff water infiltrated through karst swallow holes reached the

outlet rapidly. Meanwhile, the depletion of $\delta^{18}O$ values observed in the spring water in some flood events is smoothed when compared with the isotopic variations of recharge rainwater. This indicates the mixing of recently infiltrated water (i.e. via conduit flow) with groundwater previously stored in the saturated zone, whose isotopic signal is close to that of the weighted mean values of precipitation (Fig. 3 & 4). Similarly, the rise of the ^{3}H activity registered after the flow peaks (sample Nº 5, Figs. 2 & 6), with values close to those of precipitation (Gil-Márquez, 2018; Castaño & Rodríguez-Arévalo, 2019), in addition to a decrease of water temperature and mineralization, is the result of the arrival of infiltrated water through the karst network. In turn, the temporal evolution of NO_3^- contents observed in the spring water (Fig. 3 & 4) could be related to the seasonal fertilization cycle of the olive orchards. The use of N-fertilizers in the area partially occurs in autumn, and may be linked to the increases of NO_3^- concentration in the floods registered in November 2014 and December 2016. However, in other flood events, NO_3^- contents vary differently, even dilutes. The runoff water that infiltrates through the swallow holes would have previously washed out part of the NO_3^- from the soil. Hence, lower or no NO_3^- content is mobilized in subsequent recharge events if no additional fertilization is applied. Despite NO_3^- having a clear origin at the surface, it cannot be properly used as soil tracer without precisely knowing the fertilization practices in the study area.

However, the arrival of recently infiltrated flows to the spring does not occur at the beginning of the floods, but after a rise in mineralization. The recharge through swallow holes initially mobilized groundwater with higher temperatures (up to 3.5°C above the mean annual air temperature) and mineralization, particularly Na^+, Cl^-, K^+, and HCO_3^-, as deduced from the temporal evolution (Fig. 4) and the PCA (Fig. 5). Such hydrochemical behavior is associated with a piston-flow effect, which has been documented in other evaporite karst springs (Chiesi et al., 2010; Frank et al., 2019). This means that groundwater previously stored in the saturated zone of the system (having higher temperature and mineralization) is mobilized and drained

561 through the outlet, as a consequence of the pressure transfer derived from the hydraulic head
562 rise produced by the recharge event. A long water-rock interaction within the system under
563 saturated conditions could explain the rise of mineralization, as suggested by the observed drop
564 of ^{3}H in piston-flow effect (sample Nº4, Figs. 2 & 6). An arrival of groundwater recharged
565 before 1953 (i.e. tritium free), may have caused the descent of ^{3}H activity at the spring. The
566 increase in temperature, in turn, might be related to the ascending of deeper groundwater flows.
567 In a previous tracing experiment (Gil-Márquez et al., 2017a), it was demonstrated that artificial
568 dyes injected at the beginning of the recharge event reached the spring when mineralization and
569 water temperature had begun to decrease, after the piston-flow effect. Afterwards, the arrival
570 of recently infiltrated groundwater to the spring, via the karst conduit network, would give rise
571 to the onset of chemical dilution and cooling of the water drained by the Lower Anzur spring.
572 The lag-time observed from the flow peaks to the minimum values of mineralization (from 2 to
573 6 days, Figs. 3 & 4) can be attributed to the delay between the pressure head transfer —which
574 causes the discharge peak— and arrival to the outlet of fresh recharge water from the surface,
575 via the karst network, leading to dilution of the spring water. The lag would also be conditioned
576 by the hydrodynamic state of the system prior to the recharge event.

577 The joint representation of the variations of EC and discharge during unitary flood events
578 draws counter-clockwise cycles (Fig. 7) that help one understand the functioning of the system
579 drained by the Lower Anzur spring. Regardless of the magnitude of the flow peak, the initial
580 increase in discharge rate is accompanied by slight rises in EC values, accompanied by
581 increases in water temperature (Figs. 3, 4 & 7). This process (piston flow-effect) approximately
582 coincides with flow peaks in medium magnitude floods (Q = 35-70 l/s), like the one observed
583 in February 2016 (Fig. 7), followed by a rapid decrease in mineralization and a more moderate
584 recession. In contrast, during the greatest flood events with flattened hydrograph peaks
585 (Q>70l/s), like the one registered in November 2015 (Figs 4 & 7), the discharge rate continued

to increase after the piston-flow effect, yet more gently, contrary to EC and temperature values, which began to fall. This pattern is most likely linked to the flooding of karst depressions hosting swallow holes, causing a sustained recharge over time. In both flooding events, the maximum dilutions occurred during recession, much earlier than the minimum value of temperature (at depletion), when mineralization recovered the initial values. Contrariwise, during the only flood that took place in summer (August 2017), the drop in water temperature was slight, comparable to that of a winter flood with a lower flow (February 2016), though the peak flow was much greater (Fig. 7). The key would lie in the air temperature, too high in August to allow cooling of the spring water. The decrease in water temperature in the outlet during floods is therefore due to the mixing of groundwater previously stored in the saturated zone with recent infiltrated water; and this process is partially dependent on the atmospheric temperature, in line with a rapid hydrogeological connection between the recharge area and the outlet.

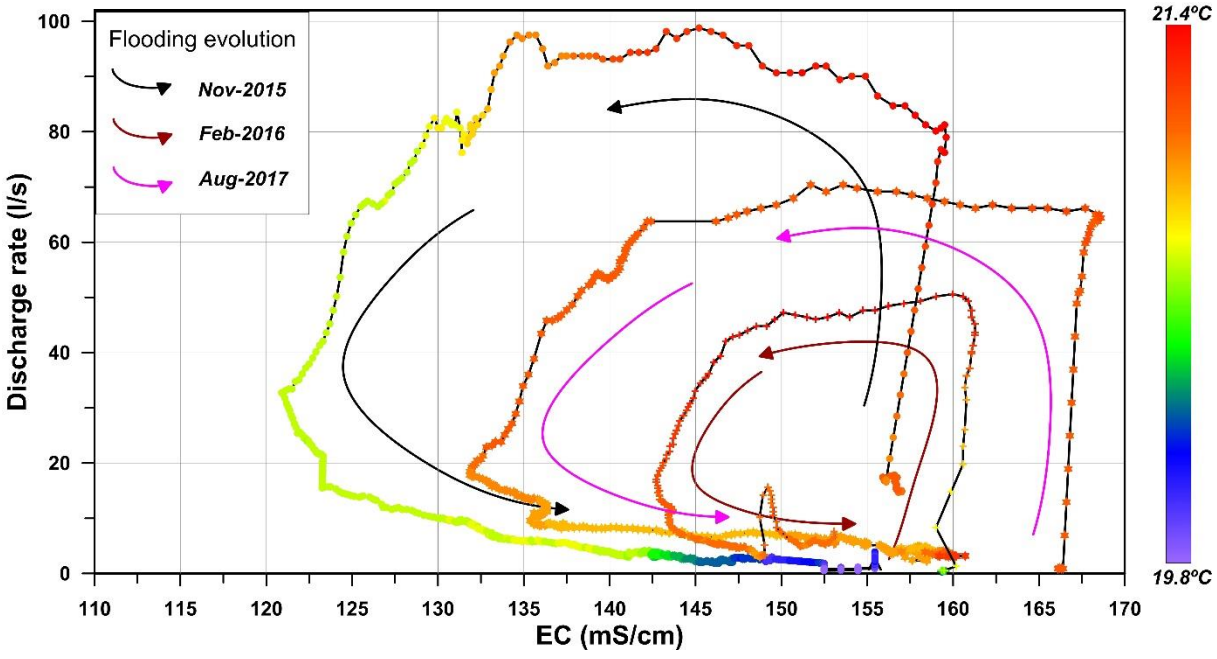

Figure 7. Hourly EC data vs discharge rate of Lower Anzur spring water during three different flood events (Nov-15, Feb-16, Aug-17). The color of each measure in the graph indicates water temperature, according to the color bar displayed on the right side, while arrows specify the temporal evolution of each flood.

The influence of air temperature in spring water was even more marked during the long-lasting recharge events that took place when the karst depressions with swallow holes were flooded. Under such conditions, the effect of recharge in the spring water temperature was lagged until the end of the recession, as seen for November 2015, December 2016, and August 2017 (Figs. 4 & 7). Nonetheless, because the groundwater flow slows down towards the end of the recession phase, the recently infiltrated water could dissolve higher solute contents given a a longer water/rock interaction. This mechanism, together with a drop of the recently infiltrated fraction in the mixed water that is drained, permits the recovery of previous EC values much sooner than the water temperature is re-established (Figs. 4 & 7).

In some carbonate karst springs, short delays of the response peaks (a few hours) of temperature with respect to those of mineralization have been reported (Birk et al., 2006; Luhmann et al., 2012; Mudarra et al., 2014), as a consequence of the lag of the heat transfer due to the interaction of water and the conduit walls (Covington et al., 2011). The process occurring in the studied system is rather peculiar, however, as the recovery of EC started several days (or even weeks) before the minimum temperature values were registered in the spring water (Fig. 4). Interpreted as a consequence of the rapid kinetics of the dissolution of evaporite minerals, this may constitute a distinctive feature of evaporitic karst systems. At any rate, such a complex process deserves investigation in further studies.

The sustained rise of temperature and mineralization throughout our study period was statistically deduced by means of the Mann-Kendall test and Sen's Slope (Tab. 3). Yet it is also visible in the right displacement of the successive EC-discharge cycles in Figure 7, as well as in the position of depletion and flood samples towards higher values of F1 and F2 in Figure 5.

During recharge episodes, the hydraulic head in the main karst conduits would be higher than in the surrounding matrix. This favors the transfer of part of the groundwater flowing through the conduit into the matrix. The later drop in the hydraulic head of the conduit network

allows groundwater stored in the matrix to flow back towards the conduits, after dissolving a greater amount of solutes. A similar process has been described in other evaporite karst areas for single flooding events (Frank et al., 2019). But the system drained by the Lower Anzur spring displays an inter-annual trend (Table 3). In wet periods, e.g. the hydrogeological years from 2009/10 to 2012/13, continuous recharge events would hardly allow the groundwater pushed into the matrix to go back to the conduit in a short time, hence the groundwater table would rise. In addition, the succession of several dry years (2013/14-2016/17) would have caused the descent of annual recharge, and therefore more and more groundwater would be displaced from the matrix to the conduits. As a result, in the mixing drained by the outlet, the fraction of water coming from the matrix of the saturated zone would gradually grow, which implies: longer residence time within the media (tritium free), higher temperature (from relatively deeper areas of the system) and mineralization. It must be underlined that there is a difference of more than 1 TU between the two depletion samples (Fig. 6). The fact that the depletion sample collected in 2015 had less ^{3}H activity than the sample of 2014 could be indicative of a higher fraction of older groundwater in the mixing, perhaps due to the reduced recharge during the study period. This interpretation is in agreement with the positive trends of mineralization and water temperature over a period of dry years. The low ^{3}H value measured in 2015 during low water conditions cannot be explained by depleted values of the historical ^{3}H in precipitation (Gil-Márquez, 2018), and therefore the existence of tritium-free groundwater in the system is certain.

The rise of mineralization is known to be a consequence of the contribution of groundwater flow of greater residence time, and is common in karst aquifers featuring evaporite layers (Wu et al., 2009; Carucci et al., 2012; Barbieri et al., 2017). Bruthans et al. (2017) studied different evaporite diapirs drained by brine spring in the Zagros Mountain Range (SW Iran). They found that ^{3}H values were lower in the outlets emplaced in diapirs where diffuse flow predominates,

654 whereas ^{3}H activity was higher in diapirs having a well-developed exokarst. Based on lumped
655 parameter models, the above authors concluded that groundwater recharged before 1950
656 dominates in the former type of diapirs.

657 The system studied in the present work is quite complex, including both conduit and diffuse
658 flow behaviors, as suggested by chemical and isotopic data (including ^{3}H). While conduit flow
659 is related to recent recharge, the spring baseflow would be associated with gravity driving
660 regional diffusive flows (Tóth, 1963; Mádl-Szőnyi & Tóth, 2015) originated by recharge
661 through permeable outcrops. If the average ^{3}H measured in precipitation (2.44 TU) is
662 considered to be representative of the younger fraction of the system, and the old component
663 has 0 TU, the mean ^{3}H activity measured in the spring water (2.00 TU; Table 1) would indicate
664 that approximately a 20% of the groundwater drained through the spring is old. The old fraction
665 would change depending on the hydrodynamic state, and could reach 55%, explaining the
666 lowest ^{3}H value measured (1.1 TU). Granted, this is a rough estimate based on very simple
667 assumptions; further attempts at groundwater dating must be performed, involving additional
668 techniques, so as to confirm the existence of the old groundwater component evoked and its
669 actual contribution.

670 Our joint analysis of the results put forth here leads us to characterize the hydrogeological
671 functioning of the system drained by the Lower Anzur spring and develop the conceptual model
672 displayed in Figure 8. It can be defined as a complex karst system in which groundwater flows
673 through conduits, but also diffusively through the clayey evaporite matrix where storage mainly
674 resides. Autogenic recharge can take place in permeable outcrops, whereas allogenic infiltration
675 via karst swallow holes plays a relevant role in feeding the system. Concentrated recharge
676 produces a pressure head transfer that mobilizes groundwater from relatively deep areas in the
677 saturated zone (warm, mineralized, of great residence time), producing a piston-flow effect.
678 The arrival of recently infiltrated groundwater to the outlet favors chemical dilution and cooling

of the groundwater drained by the spring. When a rainfall event is heavy enough (≳20 mm), the karst network becomes fully saturated and its drainage capacity is surpassed. As a consequence, runoff accumulates when reaches the swallow holes, meaning a subsequent flooding of the depressions where they are located (Fig. 8).

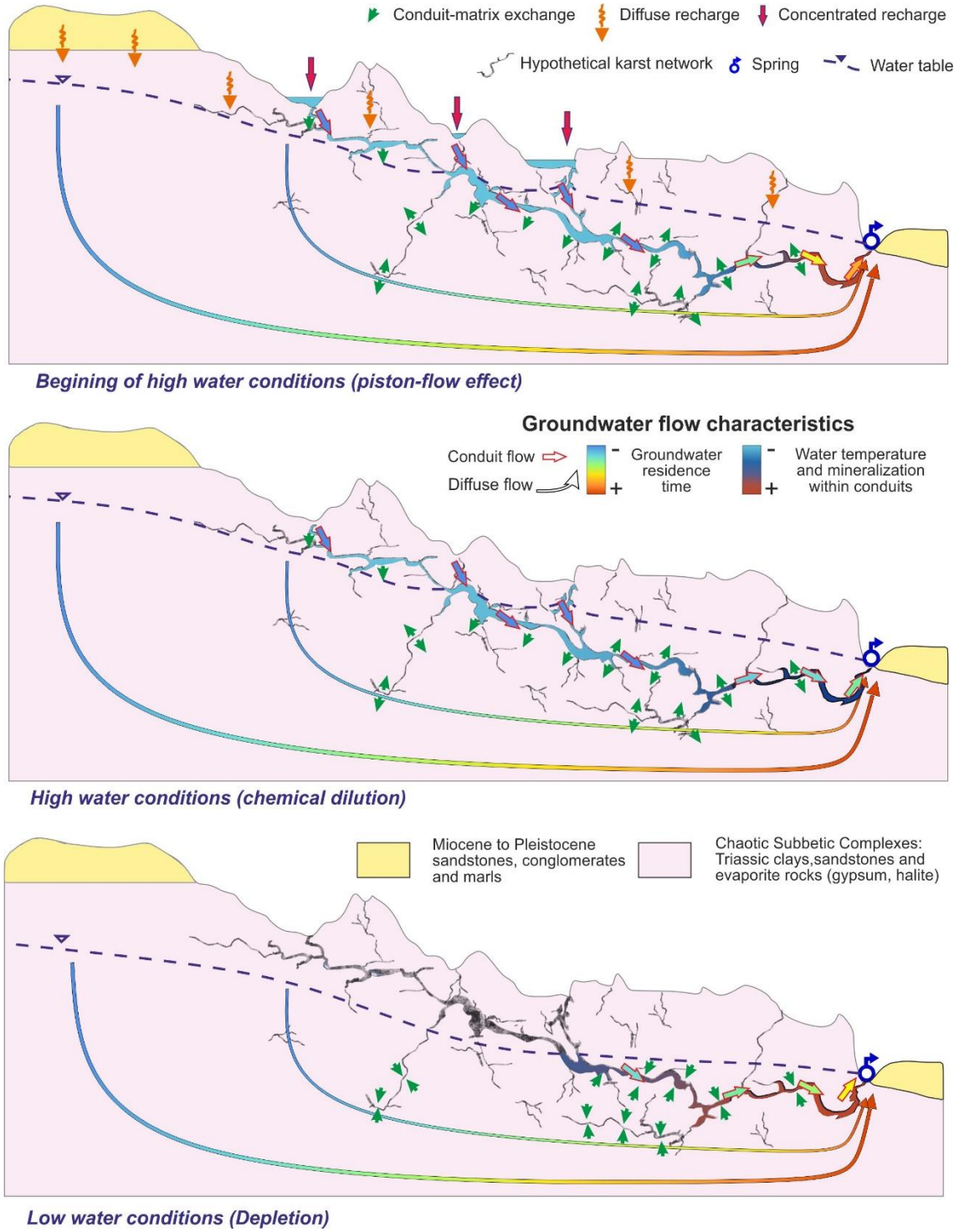

Figure 8. Hydrogeological conceptual model of the system drained through the Lower Anzur spring.

The above process provokes a long-lasting recharge, whose duration will determine the magnitude of dilutions and the length of spring floods. During wet periods, the overlap of recharge episodes would cause a situation in which the hydraulic head in the conduit network lies above the general groundwater table in the system. The latter, given the limited drainage capacity of the conduit network, would push the groundwater from the conduits into the surrounding matrix (Fig. 8). In other words, dry periods entailing fewer recharge events produce a drop of the hydraulic head, and this mobilizes the groundwater stored in the matrix; it is pushed back into the conduits, but now with higher mineralization and —if coming from deeper areas— also warmer.

In addition to the conduit flow, there must be a regional component that provides old groundwater (recharged before 1953) to the water drained at the outlet, and is responsible for the spring base flow observed in depletion times (Fig. 8). It could be traced to autogenic recharge, and would flow diffusively towards the outlet. The greater residence time of such a groundwater component in the media means a greater dissolution of solutes along its flowpath, resulting from a longer water-rock interaction than the one produced in conduits.

6. Conclusions

A multi-criteria approach combining hydrodynamic, hydrochemical, and isotopic tools has proven useful to investigate the structure and flow dynamics of evaporite karst aquifers, and may be useful in similar settings worldwide. The qualitative and statistical analyses (PCA, trend analysis) of the time series of discharge rate and physicochemical data for four years, together with the information derived from other techniques (intrinsic fluorescence, stable isotopes, tritium determination), contributed to a comprehensive knowledge of the functioning of this complex hydrogeological system. The advances presented here support a hydrogeological conceptual model to explain the observed hydrological and geochemical processes —some unlike those of traditional karst aquifers— including a faster geochemical evolution of the

recently infiltrated groundwater, local and regional flowpaths, and interaction between the matrix and conduit network. This interpretation highlights the importance of applying several methods in karst studies, and particularly in evaporite media, as altogether they permit one to focus on different areas and aspects of the systems, and then to reinforce the conclusions drawn.

Still, additional scientific efforts are needed to acquire in-depth knowledge about evaporite karst hydrogeology. Groundwater dating techniques now being applied shed light on the groundwater flowpath system inferred here, so as to quantify residence times and estimate the mixing fractions in the groundwater drained at the Lower Anzur spring. Moreover, the development of process-based karst numerical models makes it possible to simulate the natural response of the system. These recent developments in the field will serve to confirm the interpretation presented here, and define specific actions for a correct management of the water resources hosted in evaporite formations elsewhere.

7. Acknowledgments

This work is a contribution to the Excellence Projects P11-RNM-8087 and P10-RNM-6895R of the Autonomous Government of Andalusia (Spain) and to the research group RNM-308 of the Junta de Andalucía. The authors wish to thank Dr. Jo De Waele and an anonymous reviewer for their kind comments, which helped us improve the original version of the manuscript. Suggestions made by Dongmei Han as the Associated Editor are also well appreciated.

8. References

Acero, P., Auqué, L.F., Galve, J.P., Gutiérrez, F., Carbonel, D., Gimeno, M.J., Yechieli, Y., Asta, M.P., Gómez, J.B., 2015. Evaluation of geochemical and hydrogeological processes by geochemical modeling in an area affected by evaporite karstification. J. Hydrol. 529, 1874–1889. doi:10.1016/j.jhydrol.2015.07.028

734 Aghdam, J.A., Zare, M., Capaccioni, B., Raeisi, E., Forti, P., 2012. The Karun River waters in the Ambal
735 ridge region (Zagros mountain Range, southwestern Iran): Mixing calculation and hydrogeological
736 implications. Carbonates and Evaporites 27, 251–267. doi:10.1007/s13146-012-0083-8
737 Aljama Martínez A., 2017 – Sumidero de Argamasilla. Informe de cavidad. Unpublished report. Archive
738 of Grupo Espeleológico G40. Córdoba, 23 pp.
739 Andreo, B., Gil-Márquez, J.M., Mudarra, M., Linares, L., Carrasco, F., 2016. Hypothesis on the
740 hydrogeological context of wetland areas and springs related to evaporitic karst aquifers (Málaga,
741 Córdoba and Jaén provinces, Southern Spain). Environ. Earth Sci. 75, 1–19. doi:10.1007/s12665-
742 016-5545-1
743 Apaydin, A., Aktaş, S.D., 2012. Assessment of groundwater quality of the Tatlicay aquifer and relation to
744 the adjacent evaporitic formations (Cankiri, Turkey). Environ. Monit. Assess. 184, 2337–2357.
745 doi:10.1007/s10661-011-2121-8
746 Appelo, C.A.J., Postma, D., 2005. Geochemistry, Groundwater and Pollution, 2nd ed. A.A. Balkema
747 publishers, Amsterdam.
748 Bakalowicz, M., 1979. Contribution de la géochimie des eaux à la connaissance de l´aquifère karstique et
749 de la karstification. Ph.D. Thesis, Univ. París, 269 pp.
750 Barberá, J.A., Andreo, B., 2011. Functioning of a karst aquifer from S Spain under highly variable climate
751 conditions, deduced from hydrochemical records. Environ. Earth Sci. 65, 2337–2349.
752 doi:10.1007/s12665-011-1382-4
753 Barbieri, M., Nigro, A., Petitta, M., 2017. Groundwater mixing in the discharge area of San Vittorino Plain
754 (Central Italy): geochemical characterization and implication for drinking uses. Environ. Earth Sci.
755 76. doi:10.1007/s12665-017-6719-1
756 Beltram, G., 2016. Karst Wetlands, in: Finlayson, C.M., Milton, G.R., Prentice, R.C., Davidson, N.C.
757 (Eds.), The Wetland Book. Springer Science+Business Media, Dordrecht, pp. 1–16.
758 doi:10.1007/978-94-007-6173-5
759 Birdwell, J.E., Engel, A.S., 2007. Variability in Terrestrial and Microbial Contributions To Dissolved
760 Organic Matter Fluorescence in the Edwards Aquifer, Central Texas. J. Cave Karst Stud. 71, 144–
761 156.

762 Birk, S., Liedl, R., Sauter, M., 2004. Identification of localised recharge and conduit flow by combined
763 analysis of hydraulic and physico-chemical spring responses (Urenbrunnen, SW-Germany). J.
764 Hydrol. 286, 179–193. doi:10.1016/j.jhydrol.2003.09.007
765 Birk, S., Liedl, R., Sauter, M., 2006. Karst spring responses examined by process-based modeling. Ground
766 Water 44, 832–836. doi:10.1111/j.1745-6584.2006.00175.x
767 Bonacci, O., 1993. Karst springs hydrographs as indicators of karst aquifers. Hydrol. Sci. J. 38, 51–62.
768 doi:10.1080/02626669309492639
769 Bonacci, O., Bojanic, D., 1991. Rhythmic karst springs. Hydrol. Sci. J. 36, 35–47.
770 doi:10.1080/02626669109492483
771 Bruthans, J., Kamas, J., Filippi, M., Zare, M., Mayo, A.L., 2017. Hydrogeology of salt karst under different
772 cap soils and climates (Persian Gulf and Zagros Mts., Iran). Int. J. Speleol. 46, 303–320.
773 Buchignani, V., Avanzi, G.D.A., Giannecchini, R., Puccinelli, A., 2008. Evaporite karst and sinkholes: A
774 synthesis on the case of Camaiore (Italy). Environ. Geol. 53, 1037–1044. doi:10.1007/s00254-007-
775 0730-x
776 Calaforra, J.M., Pulido-Bosch, A., 1999. Gypsum karst features as evidence of diapiric processes in the
777 Betic Cordillera, Southern Spain. Geomorphology 29, 251–264.
778 Calaforra, J.M., Pulido-Bosch, A., Lopez-Chicano, M., 2002. Gypsum karst in the Betic Cordillera (south
779 Spain). Carbonates and Evaporites 17, 134–141. doi:10.1007/BF03176479
780 Calaforra, J.M., Forti, P., Fernandez-Cortes, A., 2008. Speleothems in gypsum caves and their
781 paleoclimatological significance. Environ. Geol. 53, 1099–1105. doi:10.1007/s00254-007-
782 0737-3
783 Cardona, A., Gutierrez-Ojeda, C., Martínez-Morales, M., Ortiz-Flores, G., González-Hita, L., 2018.
784 Hydrogeochemical characterization and evolution of a regional karst aquifer in the Cuatrociénegas
785 area, Mexico. Environ. Earth Sci. 77, 1–20. doi:10.1007/s12665-018-7953-x
786 Carrasco, F., 1986. Contribution to a better knowledge of the Upper Guadalhorce River Basin. Physical
787 context. Hydrochemistry Ph.D. Thesis. Univ. of Granada.

788 Carucci, V., Petitta, M., Aravena, R., 2012. Interaction between shallow and deep aquifers in the Tivoli
789 Plain (Central Italy) enhanced by groundwater extraction: A multi-isotope approach and geochemical
790 modeling. Appl. Geochemistry 27, 266–280. doi:10.1016/j.apgeochem.2011.11.007
791 Castaño, S., Rodríguez-Arevalo, J., 2019. Mapping environmental tritium activity concentration in recent
792 precipitation in Spain to trace moisture sources in the hydrological cycle, in: Proceeding of the
793 International Symposium on Isotope Hydrology. Advancing the Understanding of Water Cycle
794 Processes. Vienna, 2019
795 Chen, Z., Auler, A.S., Bakalowicz, M., Drew, D., Griger, F., Hartmann, J., Jiang, G., Moosdorf, N., Richts,
796 A., Stevanovic, Z., Veni, G., Goldscheider, N., 2017. The World Karst Aquifer Mapping project:
797 concept, mapping procedure and map of Europe. Hydrogeol. J. 25, 771–785. doi:10.1007/s10040-
798 016-1519-3
799 Chiesi, M., de Waele, J., Forti, P., 2010. Origin and evolution of a salty gypsum/anhydrite karst spring: The
800 case of Poiano (Northern Apennines, Italy). Hydrogeol. J. 18, 1111–1124. doi:10.1007/s10040-010-
801 0576-2
802 Clarke, W.B., Jenkins, W.J., Top, Z., 1976. Determination of tritium by mass-spectrometric measurement
803 of 3He. Int. J. Appl. Radiat. Isot. 27, 515–522. Doi: 10.1016/0020-708X(76)90082-X
804 Columbu, A., De Waele, J., Forti, P., Montagna, P., Picotti, V., Pons-Branchu, E., Hellstrom, J., Bajo, P.,
805 Drysdale, R., 2015. Gypsum caves as indicators of climate-driven river incision and aggradation in
806 a rapidly uplifting region. Geology 43, 539–542. doi:10.1130/G36595.1
807 Covington, M.D., Luhmann, A.J., Gabrovšek, F., Saar, M.O., Wicks, C.M., 2011. Mechanisms of heat
808 exchange between water and rock in karst conduits. Water Resour. Res. 47.
809 doi:10.1029/2011WR010683
810 D'Angeli, I.M., Serrazanetti, D.I., Montanari, C., Vannini, L., Gardini, F., De Waele, J., 2017.
811 Geochemistry and microbial diversity of cave waters in the gypsum karst aquifers of Emilia
812 Romagna region, Italy. Sci. Total Environ. 598, 538–552. doi:10.1016/j.scitotenv.2017.03.270
813 De Waele, J., Pasini, G., 2013. Intra-messinian gypsum palaeokarst in the Northern Apennines and its
814 palaeogeographic implications. Terra Nov. 25, 199–205. doi:10.1111/ter.12021

De Waele, J., Piccini, L., Columbu, A., Madonia, G., Vattano, M., Calligaris, C., D'Angeli, I.M., Parise, M., Chiesi, M., Sivelli, M., Vigna, B., Zini, L., Chiarini, V., Sauro, F., Drysdale, R., Forti, P., 2017. Evaporite karst in Italy: A review. Int. J. Speleol. 46, 137–168. doi:10.5038/1827-806X.46.2.210

Di Maggio C., Madonia G., Parise M. & Vattano M., 2012, Karst of Sicily and its conservation. Journal of Cave and Karst Studies, vol. 74 (2), p. 157-172.

Divar, J., Roldán, F.J., Molina, J.M., 1988. Geological map of Spain, sheet Nº 988 (Puente Genil). 1:50,000 scale. Instituto Geológico y Minero de España, Madrid.

EU, 1995. Hydrogeological aspects of groundwater protection in karstic areas, Final report (COST action 65). – European Commission, Directorat-General XII Science, Research and Development, Report EUR 16547 EN: 446 p.; Brussels, Luxemburg.

EU, 2004. Vulnerability and risk mapping for the protection of carbonate (karst) aquifers: final report (COST action 620). – European Commission, Directorate-General for Research, Report EUR 20912 EN: 297 p.

Fidelibus, M.D., Gutiérrez, F., Spilotro, G., 2011. Human-induced hydrogeological changes and sinkholes in the coastal gypsum karst of Lesina Marina area (Foggia Province, Italy). Eng. Geol. 118, 1–19. doi:10.1016/j.enggeo.2010.12.003

Filippini, M., Squarzoni, G., De Waele, J., Fiorucci, A., Vigna, B., Grillo, B., Riva, A., Rossetti, S., Zini, L., Casagrande, G., Stumpp, C., Gargini, A., 2018. Differentiated spring behavior under changing hydrological conditions in an alpine karst aquifer. J. Hydrol. doi:10.1016/j.jhydrol.2017.11.040

Frank, S., Goeppert, N., Ohmer, M., Goldscheider, N., 2019. Sulfate variations as a natural tracer for conduit-matrix interaction in a complex karst aquifer. Hydrol. Process. 1–12. doi:10.1002/hyp.13400

Ford, D., Williams, P., 2007. Karst Hydrogeology and Geomorphology. Chichester: John Wiley & Sons, Ltd. 562 pp.

Gil-Márquez, J.M., Barberá, J.A., Mudarra, M., Andreo, B., Prieto-Mera, J., Sánchez, D., Rizo-Decelis, L.D., Argamasilla, M., Nieto, J.M., De la Torre, B., 2017a. Karst development of an evaporitic system and its hydrogeological implications inferred from GIS-based analysis and tracing techniques. Int. J. Speleol. 46, 219–235. doi:https://doi.org/10.5038/1827-806X.46.2.2115

842 Gil-Márquez, J.M., Barberá, J.A., Andreo, B., Mudarra, M., 2017b. Hydrological and geochemical
843 processes constraining groundwater salinity in wetland areas related to evaporitic (karst) systems. A
844 case study from Southern Spain. J. Hydrol. 544, 538–554. doi:10.1016/j.jhydrol.2016.11.062
845 Gil-Márquez, J.M. 2018. Hydrogeological characterization of hypersaline wetlands and springs related to
846 evaporite karst aquifers in the Subbetic region (in Spanish). PhD Thesis. Univ. Granada, 490 pp.
847 Goldscheider, N., Drew, D., 2007. Methods in Karst Hydrogeology. Taylor & Francis, London, 264 pp.
848 Gue, A.E., Mayer, B., Grasby, S.E., 2015. Applied Geochemistry Origin and geochemistry of saline spring
849 waters in the Athabasca oil. Appl. Geochem. 61, 132–145. doi:10.1016/j.apgeochem.2015.05.015
850 Gutiérrez, F., Guerrero, J., Lucha, P., 2008a. A genetic classification of sinkholes illustrated from evaporite
851 paleokarst exposures in Spain. Environ. Geol. 53, 993–1006. doi:10.1007/s00254-007-0727-5
852 Gutiérrez, F., Calaforra, J.M., Cardona, F., Ortí, F., Durán, J.J., Garay, P., 2008b. Geological and
853 environmental implications of the evaporite karst in Spain. Environ. Geol. 53, 951–965.
854 doi:10.1007/s00254-007-0721-y
855 Gutiérrez F., Parise M., De Waele J. & Jourde H., 2014 - A review on natural and human-induced
856 geohazards and impacts in karst. Earth Sci. Rev., 138, 61-88. doi:10.1016/j.earscirev.2014.08.002.
857 Hartmann, A., Goldscheider, N., Wagener, T., Lange, J., Weller, M., 2014. Karst water resources in a
858 changing world: Review of hydrological modeling approaches. Rev. Geophys. 52, 218-242.
859 Helsel, D.R., Hirsch, R.M., 2002. Statistical methods in water resources. US Geological Survey,
860 Washington, DC. Book 4, Chapter A3.
861 Hidalgo, M.C., Cruz-Sanjulián, J., 2001. Groundwater composition, hydrochemical evolution and mass
862 transfer in a regional detrital aquifer (Baza basin, southern Spain). Appl. Geochemistry 16, 745–758.
863 doi:10.1016/S0883-2927(00)00078-0
864 Hirsch, R.M., Alexander, R.B., Smith, R.A., 1991. Selection of Methods for the Detection and Estimation
865 of Trends in Water-Quality. Water Resour. Res. 27, 803–813. doi:10.1029/91wr00259
866 Horita, J., 1989. Analytical aspects of stable isotopes in brines. Chem. Geol. 79, 107–112.
867 Hryniv, S. P., B. V. Dolishniy, O. V. Khmelevska, A. V. Poberezhskyy, and S. V. Vovnyuk, 2007,
868 Evaporites of Ukraine: a review: Geological Society, London, Special Publications, v. 285, p. 309–
869 334.

870 Hunkeler, D., Mudry, J., 2007. Hydrochemical methods. In: Goldscheider, N. & Drew, D.P. (Eds.),
871 Methods in Karst Hydrogeology. Taylor & Francis, London, 93–121 pp.
872 Johnson, K.S., 1985. Hydrogeology and Recharge of a Gypsum - Dolomite Karst Aquifer in Southwestern
873 Oklahoma, USA. Proceedings of the Ankara - Antalya, Symposium, July 1985, (161).
874 Kaçaroğlu, F., Değirmenci, M., Cerit, O., 2001.Water quality problems of a gypsiferous watershed: upper
875 Kizilirmak basin, Sivas, Turkey. Water Air Soil Pollut. 128, 161–180.
876 Kendall, M.G., 1975. Rank correlation methods, 4th ed. Charles Griffin, London
877 Klimchouk, A., 1996. Hydrogeology of gypsum formations. Int. J. Speleol. 25 (3-4), 83–89.
878 Klimchouk, A., Forti, P., Cooper, A., 1996. Gypsum karst of the World: a brief overview. Int. J. Speleol.
879 25, 159–181.
880 Klimchouk, A.B., Aksem, S.D., 2005. Hydrochemistry and solution rates in gypsum karst: case study from
881 the Western Ukraine. Environ. Geol. 48 (3), 307–319. http://dx.doi.org/10.1007/s00254-005-1277-
882 3.
883 Klimchouk, A., 2012. Gypsum caves. In: Culver, D. C., & White, W. B. 2012. Encyclopedia of caves.
884 Oxford: Elsevier, pp. 364-373.
885 LaMoreaux, P.E., 1999. The historical perspective. In: Drew, D.P. & Hötzl, H. (eds.) Karst Hydrogeology
886 and Human Activities: Impacts, Consequences, and Implications. IAH International Contributions to
887 Hydrogeology 20. Rotterdam, Balkema, pp. 13-30.
888 Lapworth, D.J., Gooddy, D.C., Allen, D., Old, G.H., 2009. Understanding groundwater, surface water, and
889 hyporheic zone biogeochemical process in a Chalk catchment using fluorescence properties of
890 dissolved and colloidal organic matter. J. Geophys. Res. Biogeosciences 114, 1–10.
891 doi:10.1029/2009JG000921
892 Lawaetz, A.J., Stedmon, C.A., 2009. Fluorescence Intensity Calibration Using the Raman Scatter Peak of
893 Water. Appl. Spectrosc. 63, 936–940.
894 Luhmann, A.J., Covington, M.D., Alexander, S.C., Chai, S.Y., Schwartz, B.F., Groten, J.T., Alexander,
895 E.C., 2012. Comparing conservative and nonconservative tracers in karst and using them to estimate
896 flow path geometry. J. Hydrol. 448–449, 201–211. doi:10.1016/j.jhydrol.2012.04.044

Mádl-Szőnyi, J., Tóth, Á. 2015. Basin-scale conceptual groundwater flow model for an unconfined and confined thick carbonate region. Hydrogeol. J. 23, 1359–1380. doi:10.1007/s10040-015-1274-x

Malard, A., Jeannin, P.Y., Weber, E., 2015. Assessing the Contribution of Karst to Flood Peaks of the Suze River, Potentially Affecting the City of Bienne (Switzerland), in: Lollino, G. et al. (Ed.), Engineering Geology for Society and Territory - Volume 3. pp. 175–180. doi:10.1007/978-3-319-09408-3

Mann, H.B., 1945. Non parametric tests against trend. Econometrica 13, 245–259.

Martín-Serrano, A., 1986. Geological map of Spain, sheet Nº 1006 (Benamejí). 1:50,000 scale. Instituto Geológico y Minero de España, Madrid.

Mehta, S., Fryar, A.E., Brady, R.M., Morin, R.H., 2000. Modeling regional salinization of the Ogallala aquifer, Southern High Plains, TX, USA. J. Hydrol. 238, 44–64. doi:10.1016/S0022-1694(00)00314-0

Melloul. A., Collin, M., 1992. The principal components statistical method as a complementary approach to geochemical methods in water quality factor identification: application to the Coastal Plain aquifer of Israel. J. Hydrol. 140, 49–73.Memon, B.A., Patton, A.F., Pitts, M.W., 1999. Control of naturally occurring brine springs and seeps in an evaporite karst setting. Eng. Geol. 52, 83–91. doi:10.1016/S0013-7952(98)00058-1

Merchán, D., Causapé, J., Abrahão, R., 2013. Impact of irrigation implementation on hydrology and water quality in a small agricultural basin in Spain. Hydrol. Sci. J. 58, 1400–1413. doi:10.1080/02626667.2013.829576

Miyamoto, S., Yuan, F., Anand, S., 2007. Water balance, salt loading, and salinity control options of Red Bluff Reservoir, Texas. El Paso. Texas A&M University Agricultural Agricultural Experiment Research Center al El Paso. TR-298, 40pp.

Mucci, A., 1983. The solubility of calcite and aragonite in seawater at various salinities, temperatures, and one atmosphere total pressure. Am. J. Science 283, 780–799.

Mudarra, M., Andreo, B., Baker, A., 2011. Characterisation of dissolved organic matter in karst spring waters using intrinsic fluorescence: Relationship with infiltration processes. Sci. Total Environ. 409, 3448–3462. doi:10.1016/j.scitotenv.2011.05.026

924 Mudarra, M., Andreo, B., Marín, A.I., Vadillo, I., Barberá, J.A., 2014. Combined use of natural and
925 artificial tracers to determine the hydrogeological functioning of a karst aquifer: the Villanueva del
926 Rosario system (Andalusia, southern Spain). Hydrogeol. J. 22, 1027–1039. doi:10.1007/s10040-014-
927 1117-1
928 Mudry, J., Blavoux, B., 1986. Utilisation de l'analyse en composantes principales (sur variables centrées
929 réduites) pour l'étude du fonctionnement hydrocinématique de trois aquifères karstiques du Sud-Est
930 de la France. Hydrogéologie 1, 53–59.
931 Naderi, M., Raeisi, E., Zarei, M., 2016. The impact of halite dissolution of salt diapirs on surface and ground
932 water under climate change, South-Central Iran. Environ. Earth Sci. 75, 708. doi:10.1007/s12665-
933 016-5525-5
934 Négrel, P., Roy, S., Petelet-giraud, E., Millot, R., Brenot, A., 2007. Long-term fluxes of dissolved and
935 suspended matter in the Ebro River Basin (Spain). J. Hydrol., *342*, 249–260.
936 http://doi.org/10.1016/j.jhydrol.2007.05.013
937 Nekouei, E., Zarei, M., 2017. Karst hydrogeology of Karmustadj salt diapir, southern Iran. Carbonates and
938 Evaporites 32, 315–323. doi:10.1007/s13146-016-0298-1
939 Omelon, C.R., Pollard, W.H., Andersen, D.T., 2006. A geochemical evaluation of perennial spring activity
940 and associated mineral precipitates at Expedition Fjord, Axel Heiberg Island, Canadian High Arctic.
941 Appl. Geochemistry 21, 1–15. doi:10.1016/j.apgeochem.2005.08.004
942 Parise, M., Trocino, A., 2005. Gypsum karst in the Crotone province (Calabria, Southern Italy). Acta
943 carsologica 34, 369–382.
944 Parise, M., Qiriazi, P., Sala, S., 2008. Evaporite karst of Albania: Main features and cases of environmental
945 degradation. Environ. Geol. 53, 967–974. doi:10.1007/s00254-007-0722-x
946 Parise M., 2010, Hazards in karst. In: Bonacci O. (Ed.), Proceedings International Interdisciplinary
947 Scientific Conference "Sustainability of the karst environment. Dinaric karst and other karst regions",
948 Plitvice Lakes (Croatia), 23-26 September 2009, IHP-UNESCO, Series on Groundwater no. 2, p.
949 155-162.
950 Parise, M., Sammarco, M., 2015. The historical use of water resources in karst. Environ. Earth Sci.
951 74, 143–152. doi:10.1007/s12665-014-3685-8

952 Parkhurst, D.L., Appelo, C.A.J., 2013. Description of input and examples for PHREEQC version 3 – a
953 computer program for speciation, batch-reaction, one-dimensional transport, and inverse
954 geochemical calculations. U.S. Geological Survey Techniques and Methods 6–A43; 2013.
955 Pérez-López, A., Sanz de Galdeano, C. 1994. Tectónica de los materiales triásicos en el sector central de
956 la Zona Subbética (Cordillera Bética). Revista de La Sociedad Geológica de España, *7*(1–2), 141–
957 153.
958 Phillips, F.M., Mills, S., Hendrickx, M.H., Hogan, J., 2003. Environmental Tracers Applied to Quantifying
959 Causes of Salinity in Arid-Region Rivers: Results from the Rio Grande Basin, Southwestern USA,
960 in: Alsharhan, A.S., Wood, W.W. (Eds.), Water Resources Perspectives: Evaluation, Management
961 and Policy. Elsevier Science, Amsterdam, pp. 327–334.
962 Plummer, L.N., Parkhurst, D.L., Fleming, G.W., Dunkle, S.A., 1988. A computer program incorporating
963 Pitzer's equations for calculation of geochemical reactions in brines. Water-Resour. Invest. Report,
964 88–4153.
965 Pulido-Bosch A., Calaforra J.M. 1993. The gypsum karstic aquifer of Sorbas (Almeria). In: Pulido-Bosch
966 A. (Ed.). Some Spanish karstic aquifers. Universidad de Granada, pp. 225-241.
967 Qi, J., Li, X., Xu, M., Yi, L., Zhang, Q., Qin, L., Li, K., 2018. Applied Geochemistry Origin of saline
968 springs in Yanjing, Tibet : Hydrochemical and isotopic characteristics. Appl. Geochemistry 96, 164–
969 176. doi:10.1016/j.apgeochem.2018.06.013
970 Raeisi, E., Zare, M., Aghdam, J.A., 2013. Hydrogeology of gypsum formations in Iran. J. Cave Karst Stud.
971 75, 68–80. doi:10.4311/2011ES0234
972 Reisenhofer, E., Adami, G., Barbieri, P., 1998. Using chemical and physical parameters to define the quality
973 of karstic freshwaters (Timavo River, North-eastern Italy): A chemometric approach. Water Res. 32,
974 1193–1203. doi:10.1016/S0043-1354(97)00325-4
975 Sánchez, D., Barberá, J.A., Mudarra, M., Andreo, B., 2015. Hydrogeochemical tools applied to the study
976 of carbonate aquifers: examples from some karst systems of Southern Spain. Environ. Earth Sci. 74,
977 199–215. doi:10.1007/s12665-015-4307-9
978 Sanna, L., De Waele, J., Calaforra, J.M., Forti, P., 2015. Long-term erosion rate measurements in gypsum
979 caves of Sorbas (SE Spain) by the Micro-Erosion Meter method. Geomorphology 228, 213-225.

Sathish, S., Mohamed, M., Klammler, H., 2018. Regional groundwater flow model for Abu Dhabi Emirate: scenario-based investigation. Environ. Earth Sci. 77, 0. doi:10.1007/s12665-018-7544-x

Sen, P.K., 1968. Estimates of the regression coefficient based on Kendall's tau. J. Am. Stat. Assoc. 63, 1379–1389.

Smart, C. & Worthington, S.R.H., 2004. Springs. In Gunn, J. (Ed). Encyclopedia of caves and karst science. Taylor & Francis, New York, pp. 1495-1505.

Sofer, Z., Gat, J.R., 1972. Activities and concentrations of oxygen-18 in concentrated aqueous salt solutions analytical and geophysical implications. Earth Planet. Sci. Lett. 15, 232–238.

Sofer, Z., Gat, J.R., 1975. The isotope composition of evaporating brines: effect of the isotopic activity ration in saline solutions. Earth Planet. Sci. Lett. 26, 179–186.

Stevanovic Z. (2018) Global distribution and use of water from karst aquifers. In: Parise M., Gabrovsek F., Kaufmann G. & Ravbar N. (Eds.), Advances in Karst Research: Theory, Fieldwork and Applications. Geological Society, London, Special Publications, 466, pp. 217-236.

Stuart, M.E., Chilton, P.J., Kinniburgh, D.G., Cooper, D.M., 2007. Screening for long-term trends in groundwater nitrate monitoring data. Q. J. Eng. Geol. Hydrogeol. 40, 361–376. doi:10.1144/1470-9236/07-040

Sullivan, P.L., Price, R.M., Gaiser, E.E., 2013. The Influence of Hydrologic Restoration on Groundwater-Surface Water Interactions in a Karst Wetland, the Everglades (FL, USA). Wetlands S1, 23–35. doi:10.1007/s13157-013-0451-8

Sültenfuss, J., Roether, W., Rhein, M., 2009. The Bremen mass spectrometric facility for the measurement of helium isotopes, neon, and tritium in water. Isotopes Environ. Health Stud. 45, 83–95. doi:10.1080/10256010902871929

Taube, H. 1954. Use of oxygen isotope effects in the study of hydratation of ions. J. Phys. Chem. 58: 532-528.

Tóth, J., 1963. A Theoretical Analysis of Groundwater Flow in Small Drainage Basins. J. Geophys. Res. 68, 4795–4812. doi:10.1029/JZ068i016p04795

Urresti-Estala, B., Gavilán, P.J., Vadillo, I., Carrasco, F., 2016. Assessment of hydrochemical trends in the highly anthropised Guadalhorce River basin (southern Spain) in terms of compliance with the

European groundwater directive for 2015. Environ. Sci. Pollut. Res. 23, 15990–16005. doi:10.1007/s11356-016-6662-9

Valero-Garcés, B.L., González-Sampériz, P., Navas, A., Machín, J., Mata, P., Delgado-Huertas, A., Bao, R., Moreno, A., Carrión, J.S., Schwalb, A., González-Barrios, A., 2006. Human impact since medieval times and recent ecological restoration in a Mediterranean lake: The Laguna Zoñar, southern Spain. J. Paleolimnol. 35, 441–465. doi:10.1007/s10933-005-1995-2

Velaj, T., 2002. Evaporites in Albania and their impact on the thrusting processes. Carbonates and Evaporites 17, 68–78. doi:10.1007/BF03175658

Vera, J.A., Martín-Algarra, A., 2004. Cordillera bética. In: Vera, J.A. (Ed.), Geología de España. IGME-Sociedad Geológica de España, Madrid, pp. 345–464.

Vigna, B., D'Angeli, I.M., Fiorucci, A., De Waele, J., 2017. Hydrogeological flow in gypsum karst areas: Some examples from northern Italy and main circulation models. Int. J. Speleol. 46, 205–217. doi:10.5038/1827-806X.46.2.2095

Wahlin, K., Grimvall, A., 2010. Roadmap for assessing regional trends in groundwater quality. Environ. Monit. Assess. 165, 217–231. doi:10.1007/s10661-009-0940-7

Warren, J. K., 2016. Evaporites. A geological Compendium. Heidelberg: Springer. 1813 pp.

Wigley, T.M.L., 1973. Chemical evolution of the system calcite-gypsum-water. Can. J. Earth Sci. 10 (2), 306–315.

Wu, P., Tang, C., Zhu, L., Liu, C., Cha, X., Tao, X., 2009. Hydrogeochemical characteristics of surface water and groundwater in the karst basin, southwest China. Hydrol. Process. 23, 2012–2022. doi:10.1002/hyp.7332

Yechieli, Y., Abelson, M., Baer, G., 2016. Sinkhole formation and subsidence along the Dead Sea coast, Israel. Hydrogeol. J. 24, 601–612. doi:10.1007/s10040-015-1338-y

Yue, S., Wang, C.Y., 2004. The Mann-Kendall test modified by effective sample size to detect trend in serially correlated hydrological series. Water Resour Manag 18:201–218